Multiphysics Simulation Environments for Shell and Spatial Structures

Session Organizers: Fehmi CIRAK (University of Cambridge), Ekkehard RAMM (Stuttgart University)

Keynote Lecture
Advanced approaches for fluid-shell interaction
Wolfgang A. WALL, Axel GERSTENBERGER, Ursula M. MAYER, Ulrich KÜTTLER (TU Munich)*

Numerical simulation of fluid-structure interaction for wind-induced dynamic response of the 3rd Jinan Yellow River cable-stayed bridge
Qi-Lin ZHANG, Zhen-Hua LIU (Tongji University), Ying ZHOU (Shandong University)*

A consistent finite element approximation for piezoelectric shell structures
Dieter LEGNER, Sven KLINKEL, Werner WAGNER (University of Karlsruhe)*

Vibration analysis of thin-walled – gas or fluid filled – structures including the effect of the inflation/filling process
Karl SCHWEIZERHOF, Marc HAßLER (University of Karlsruhe)*

Thin-walled structures interacting with incompressible flows
Ekkehard RAMM, Malte VON SCHEVEN (University of Stuttgart), Christiane FÖRSTER, Wolfgang A. WALL (TU Munich)*

Full SPH modeling of the dynamic failure of shells filled with a fluid
Alain COMBESCURE (LaMCoS), Farid ABED MERAIM (LPMM), Bertrand MAUREL (LaMCoS)*

Fluid-shell coupled simulation of supersonic disk-gap-band parachutes
Konstantinos KARAGIOZIS, Ramji KAMAKOTI, Carlos PANTANO (University of Illinois at Urbana-Champaign), Fehmi CIRAK (University of Cambridge)*

Strongly coupled approach for the treatment of the fluid-structure interaction problems involving highly deformable solids and shells
Riccardo ROSSI, P. RYZHAKOV, Eugenio OÑATE (CINME, UPC)*

Numerical simulation of fluid-structure interaction for wind-induced dynamic response of cylindrical steel tanks with a dome roof
Qi-Lin ZHANG, Zhen-Hua LIU (Tongji University), Ying ZHOU (Shandong University)*

For multiple-author papers:
Contact author designated by *
Presenting author designated by underscore

Proceedings of the 6th International Conference on
Computation of Shell and Spatial Structures
IASS-IACM 2008: "Spanning Nano to Mega"
28-31 May 2008, Cornell University, Ithaca, NY, USA
John F. ABEL and J. Robert COOKE (eds.)

Advanced approaches for fluid-shell interaction

Wolfgang A. WALL*, Axel GERSTENBERGER[1], Ursula M. MAYER, Ulrich KÜTTLER

Chair for Computational Mechanics
Technical University of Munich
Boltzmannstrasse 15, 85748 Garching, Germany
e-mail: wall@lnm.mw.tum.de - Web page: http://www.lnm.mw.tum.de/

Abstract

Fluid-structure interaction is especially challenging when thin, light-weight structures have to be coupled to incompressible flows, which makes this topic still a very active area of research. In this talk we will present some of our recent advances in the development of general, robust, efficient and accurate approaches to tackle this problem class. Besides referring to classical Arbitrary- Lagrangean-Eulerian (ALE) based formulations we will mainly cover a new fixed-grid approach for fluid-structure interaction [2] that is able to avoid limitations most existing fixed-grid approaches are suffering from so far [6]. We will demonstrate our recent advances in the development of this approach and show the individual building blocks needed to empower this approach to deal with thin-walled structures as well as realistic three-dimensional fluid-structure interaction examples.

1. Introduction

For fluid-structure interaction problems involving large deformations, so called Eulerian / fixed-grid methods are a valuable alternative approach. When treating a structure on a fixed-fluid grid, the fluid-structure interface essentially divides the fluid domain in a physical flow field and a fictitious field that may be discretized and solved, but has no physical meaning to the FSI problem. The main challenges are the removal of the effect of the fictitious domain and the clear definition of an interface that can be coupled to the structural surface [2].

For realistic three-dimensional simulations, many more challenges have to be met. These are among others: - to realize appropriate fluid meshes (like boundary layer meshes) where needed [1]; - to locate the interface and to intersect fluid elements with structural elements – this should be possible also for higher order fluid elements and for curved structural elements [5]; - to establish an appropriate Lagrange Multiplier formulation in such a context; - to find suitable ways for intersected domain and surface integration; and to set all these algorithms up in a parallel environment that is needed for 3-dimensional large scale problems. And last but not least one also desperately needs proper coupling schemes [3, 4] in order to get an efficient overall approach.

For that purpose, we derive a 3-field FSI approach with an intermediate reference field. The 3-field approach greatly increases the flexibility with respect to discretization techniques and code modularity. Subsequently, we derive the treatment of the moving boundary on the fixed-fluid grid and its coupling to the interface. Eventually, the fluid with the moving boundary formulations can be embedded into the FSI framework used already for ALE computations.

2. Coupled Fluid-Structure Problem as a 3-Field-Problem

For maximum flexibility with respect to choice of approximation functions, mesh size and solution techniques, we propose a 3-field setup, where fluid and structural fields and an independent interface field are treated separately. This setup – along with the respective variables living on these fields or interfaces – is shown in the upper part of Fig. 1. For the 3-field problem, the kinematic interface condition ('no-slip') is given as $\boldsymbol{u} = \dot{\boldsymbol{d}}^{\mathrm{i}}$ and $\dot{\boldsymbol{d}}^{\mathrm{i}} = \dot{\boldsymbol{d}}^{\mathrm{s}}$. Let $\boldsymbol{\lambda}$

[1]Support by the German Science Foundation / Deutsche Forschungsgemeinschaft (DFG) is gratefully acknowledged.

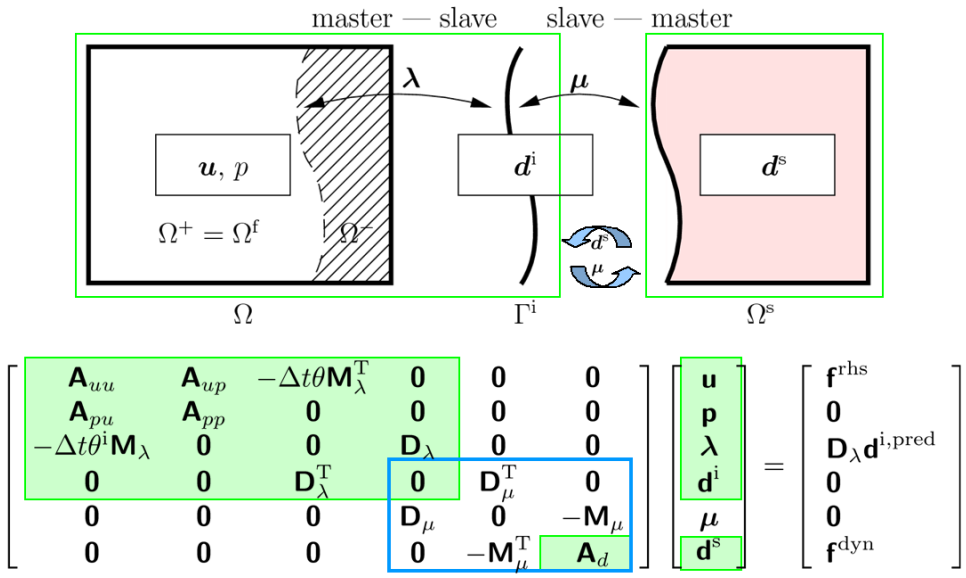

Figure 1: Iterative coupling scheme between fluid with moving interface and the structural surface (see also [2]).

and $\boldsymbol{\mu}$ be two traction fields on the interface Γ^{i} such that $\underline{\underline{\boldsymbol{\sigma}}}^{\mathrm{f}} \cdot \boldsymbol{n}^{\mathrm{f}} = \boldsymbol{\lambda}$ and $\underline{\underline{\boldsymbol{\sigma}}}^{\mathrm{s}} \cdot \boldsymbol{n}^{\mathrm{s}} = \boldsymbol{\mu}$. Then the interface traction balance can be stated as $\boldsymbol{\lambda} = -\boldsymbol{\mu}$.

Since we generally assume that neither fluid nor structural discretization match the interface mesh, we need to couple three non-fitting meshes. The single fields can be described separately using the coupling of each field to the interface.

3. Moving Fluid Boundaries and Interfaces on Fixed Eulerian Grids

Instead of formulating the fluid problem only in Ω^{f}, we introduce a discontinuous velocity and pressure field $\boldsymbol{u}$ and p in a domain Ω, such that the flow in $\Omega^+ = \Omega^{\mathrm{f}}$ corresponds to the physical flow and the fictitious flow in Ω^- remains zero at all times. The principle setup of the proposed approach is depicted on the upper left side in Fig. 1. The fluid-structure interface condition is enforced weakly using a test function $\delta\boldsymbol{\lambda}$ along the interface as

$$\left(\boldsymbol{v}, \rho^{\mathrm{f}}\dot{\boldsymbol{u}} + \rho^{\mathrm{f}}\boldsymbol{u}\cdot\boldsymbol{\nabla}\boldsymbol{u}\right)_{\Omega} + \left(\boldsymbol{\nabla}\cdot\boldsymbol{v}, -p\boldsymbol{I} + \underline{\underline{\boldsymbol{\tau}}}^{\mathrm{f}}\right)_{\Omega} + \left(q, \boldsymbol{\nabla}\cdot\boldsymbol{u}\right)_{\Omega} - \left(\boldsymbol{v}, \boldsymbol{\lambda}\right)_{\Gamma^+} - \left(\delta\boldsymbol{\lambda}, \boldsymbol{u} - \bar{\boldsymbol{u}}^{\mathrm{i}}\right)_{\Gamma^+} = 0 \qquad (1)$$

In the above weak form of the Navier-Stokes equation, $\underline{\underline{\boldsymbol{\tau}}}^{\mathrm{f}}$ denotes the viscous fluid stress tensor, p the fluid pressure and ρ^{f} the fluid density. The Lagrange multiplier field $\boldsymbol{\lambda}$ is the corresponding surface traction due to the weakly enforced Dirichlet condition.

The discontinuous velocity and stress field are employed by using the XFEM to embed the discontinuities of the primary variables and their derivatives into the shape functions

$$\boldsymbol{u}^{\mathrm{h}}(\boldsymbol{x}, t) = \sum_{I} N_I(\boldsymbol{x})\Big(\tilde{\boldsymbol{u}}_I + \psi(\boldsymbol{x}, t)\hat{\boldsymbol{u}}_I\Big) \qquad (2)$$

Here, $\tilde{\boldsymbol{u}}_I$ represent the standard nodal degrees of freedom at node I, while additional degrees of freedom $\hat{\boldsymbol{u}}_I$ multiplied by a properly chosen enrichment function $\psi(\boldsymbol{x}, t)$ are used to enhance the solution. For our purpose, we use a modified Heaviside function that is equal to 1 in Ω^+ and zero in Ω^-. With the help of this Heavyside function, most nodes and elements inside the hole can be removed resulting in savings in computation time.

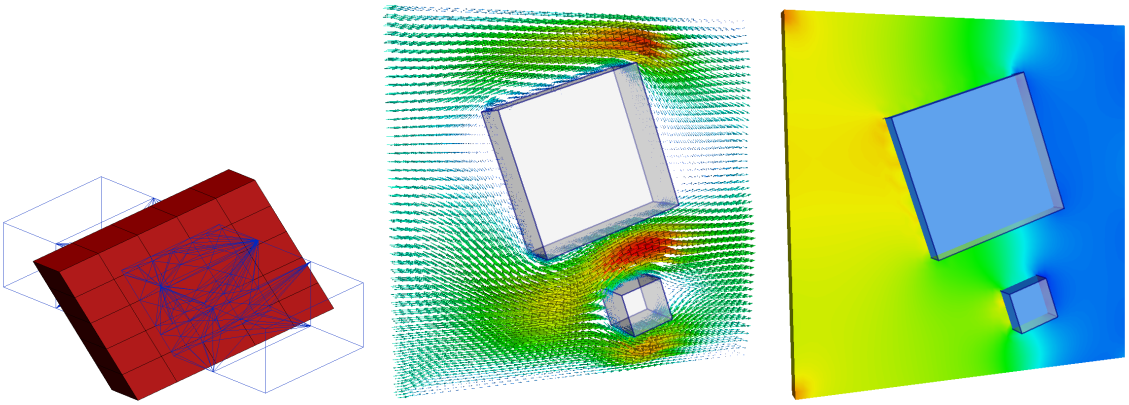

(a) intersection of fluid elements (blue) by several structural surface elements (red)

(b) velocity field

(c) pressure field

Figure 2: Example of an intersected and tetrahedralized fluid mesh and preliminary three-dimensional computations of a stationary flow around two structures. Note that only two fluid element layers are shown.

As mentioned in the Introduction, several challenges have to be met, when the presented two-dimensional formulation is extended to three-dimensional applications. Fig. 2 shows preliminary three-dimensional computations and an example of intersected fluid elements after the necessary tetrahedralization.

4. Direct Structure-Interface Coupling

For the structure-interface coupling, we adopt Mortar methods for non-matching grids. In the Mortar method, the kinematic matching condition is enforced weakly by using a Lagrange multiplier field $\boldsymbol{\mu}$, which again can be identified as a surface traction. The setup for the structure-interface coupling is depicted in the upper-right side of Fig. 1. The resulting weak form, where $\boldsymbol{d}^{\mathrm{s}}$ denotes the displacement and $\underline{\underline{\boldsymbol{\sigma}}}^{\mathrm{s}}$ the Cauchy stress, is

$$(\delta\boldsymbol{d}^{\mathrm{s}}, \rho^{\mathrm{s}}\ddot{\boldsymbol{d}}^{\mathrm{s}})_{\Omega^{\mathrm{s}}} + (\boldsymbol{\nabla}\delta\boldsymbol{d}^{\mathrm{s}}, \underline{\underline{\boldsymbol{\sigma}}}^{\mathrm{s}})_{\Omega^{\mathrm{s}}} - (\delta\boldsymbol{d}^{\mathrm{s}}, \boldsymbol{\mu})_{\Gamma^{\mathrm{i}}} - (\delta\boldsymbol{\mu}, \boldsymbol{d}^{\mathrm{s}} - \boldsymbol{d}^{\mathrm{i}})_{\Gamma^{\mathrm{i}}} = 0 \tag{3}$$

The algorithmic implementation of the coupled problem of fluid-structure interaction is based on a field-wise partitioned solution approach, where each field is solved implicitly and an iterative procedure over the fields ensures convergence for the interface conditions at the new time step level. For that purpose, we eliminate the Lagrange multiplier field $\boldsymbol{\mu}$ and replace it with an iterative approach as sketched in the lower part of Fig 1.

5. Coupling Using an Intermediate ALE Field

For reliable computations of realistic problems, one can use the presented approach to derive a coupling between a fixed fluid mesh and a moving fluid mesh. Instead of coupling the structural surface directly to the moving interface, the deformable structure is surrounded with a body fitted ALE-fluid field, which provides a straightforward way to use optimal fluid meshes near the structural surface to resolve boundary layers. The presented 3-field coupling is then performed between the fluid on the moving ALE mesh (superscript M) and the already described fixed fluid grid using the very same discontinuous velocity and pressure fields as before. With the additional grid velocity $\boldsymbol{u}^{\mathrm{G}}$, the weak form is given as

$$\begin{aligned}
&\left(\boldsymbol{v}, \rho^{\mathrm{f}}\dot{\boldsymbol{u}} + \rho^{\mathrm{f}}\boldsymbol{u}\cdot\boldsymbol{\nabla}\boldsymbol{u}\right)_{\Omega} + \left(\boldsymbol{\nabla}\cdot\boldsymbol{v}, -p\boldsymbol{I} + \underline{\underline{\boldsymbol{\tau}}}^{\mathrm{f}}\right)_{\Omega} + \left(q, \boldsymbol{\nabla}\cdot\boldsymbol{u}\right)_{\Omega} \\
+\left(\boldsymbol{v}^{\mathrm{M}}, \rho^{\mathrm{f}}\dot{\boldsymbol{u}}^{\mathrm{M}} + \rho^{\mathrm{f}}(\boldsymbol{u}^{\mathrm{M}} - \boldsymbol{u}^{\mathrm{G}})\cdot\boldsymbol{\nabla}\boldsymbol{u}^{\mathrm{M}}\right)_{\Omega^{\mathrm{M}}} &+ \left(\boldsymbol{\nabla}\cdot\boldsymbol{v}^{\mathrm{M}}, -p^{\mathrm{M}}\boldsymbol{I} + \underline{\underline{\boldsymbol{\tau}}}^{\mathrm{f,M}}\right)_{\Omega^{\mathrm{M}}} + \left(q^{\mathrm{M}}, \boldsymbol{\nabla}\cdot\boldsymbol{u}^{\mathrm{M}}\right)_{\Omega^{\mathrm{M}}} \\
&-\left(\boldsymbol{v}, \boldsymbol{\lambda}\right)_{\Gamma^{+}} - \left(\delta\boldsymbol{\lambda}, \boldsymbol{u} - \boldsymbol{u}^{\mathrm{M}}\right)_{\Gamma^{+}} + \left(\boldsymbol{v}^{\mathrm{M}}, \boldsymbol{\lambda}\right)_{\Gamma^{+}} = 0
\end{aligned} \tag{4}$$

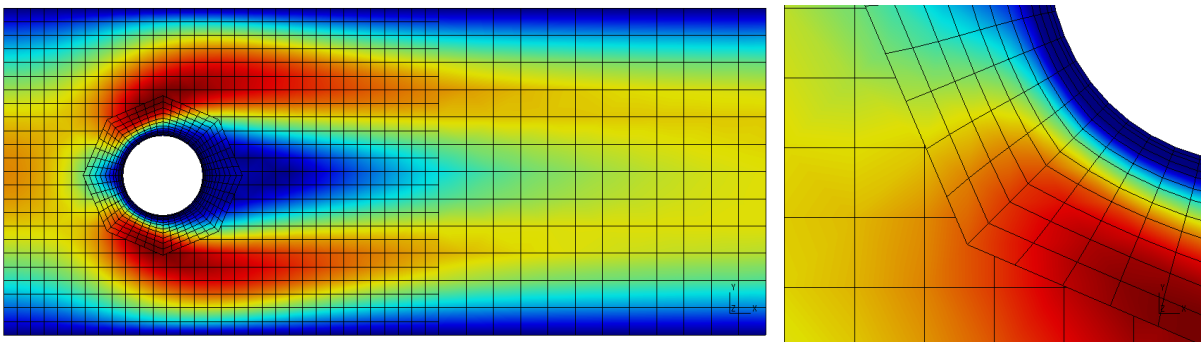

Figure 3: Coupling between a moving and a fixed fluid grid. The moving grid is aligned with the cylinder surface to resolve the boundary layer.

Both fluid fields are solved together in a monolithic way. The FSI coupling between the structure and the ALE mesh can be performed using existing monolithic or iterative Dirichlet-Neumann schemes. An example of such a fluid-fluid coupling is shown in Fig. 3.

6. Conclusions

Main improvements compared to most existing fixed-grid methods are the complete removal of the fictitious domain including its degrees of freedom and a sharp interface description. Physical and fictitious domains are completely decoupled using an eXtended Finite Element Formulation (XFEM). With multiple enrichments also very thin structures – even thinner than one underlying fluid element – can be treated easily. Due to a 3-field approach, the treatment of the structure is entirely independent of any internals of the fluid XFEM discretization.

REFERENCES

[1] A. Gerstenberger, W. A. Wall, Efficient treatment of moving interfaces on fixed grids for surface coupled problems, International Journal for Numerical Methods in Fluids, accepted, DOI: 10.1002/fld.1782.

[2] A. Gerstenberger, W. A. Wall, An extended finite element method/Lagrange multiplier based approach for fluid-structure interaction, Computer Methods in Applied Mechanics and Engineering 197 (19-20) (2008) 1699–1714.

[3] U. Küttler, W. A. Wall, Fixed-point fluid-structure interaction solvers with dynamic relaxation, Computational Mechanics, published online (2008), DOI: 10.1007/s00466–008–0255–5.

[4] U. Küttler, W. A. Wall, Vector extrapolation for strong coupling fluid-structure interaction solvers, Journal of Applied Mechanics (2008), submitted.

[5] U. M. Mayer, A. Gerstenberger, W. A. Wall, Interface handling for three-dimensional higher-order xfem computations in fluid-structure interaction, in preparation.

[6] W. A. Wall, A. Gerstenberger, P. Gamnitzer, C. Förster, E. Ramm, Large deformation fluid-structure interaction – advances in ALE methods and new fixed grid approaches, in: H.-J. Bungartz, M. Schäfer (eds.), Fluid-Structure Interaction: Modelling, Simulation, Optimisation, LNCSE, Springer Verlag, 2006.

Proceedings of the 6th International Conference on
Computation of Shell and Spatial Structures
IASS-IACM 2008: "Spanning Nano to Mega"
28-31 May 2008, Cornell University, Ithaca, NY, USA
John F. ABEL and J. Robert COOKE (eds.)

Numerical simulation of fluid-structure interaction for wind-induced dynamic response of the 3rd Jinan Yellow River cable-stayed bridge

Qi-Lin Zhang*, Zhen-Hua Liu, Ying Zhou

*Department of Building Engineering, Tongji University, Shanghai 200092, P.R.China
zhangqilin@mail.tongji.edu.cn

Abstract

The bridge aerodynamic design has considerably progressed to a more and more analytical methodology by which the mechanical aspects concerning bridge stability are deeply understood and characterized. In this paper, a response analysis was carried out using ADINA to evaluate wind-induced dynamic response of the 3rd Jinan Yellow River cable-stayed steel box girder bridge. The wind induced dynamic coefficients and the wind pressure distribution coefficient of the steel box girder can be calculated.

1. Introduction

Recently, long-span bridges become popular around the world. Long-span bridges are slender, light and flexible large-scale structures with deck dimensions very small compared to the main span length. Owing to their high flexibility, long-span bridges are often found very susceptible to wind effects.

The wind tunnel experimental data is often referenced in the bridge aerodynamic design (Zhengqing Chen [1]). This paper will present a numerical simulation of fluid-structure interaction for wind-induced dynamic response of the bridge. The method of numerical simulation can avoid the high cost of the wind tunnel experiments. Presently, many researches concentrated on the simple two-dimensional model in which only the cross-section of the cable-stayed bridge is simulated. This paper presents a numerical simulation of fluid-structure interaction for wind-induced dynamic response of a three-dimensional bridge model.

Numerical simulations of fluid flows interacting with dynamically moving boundaries are amongst the most challenging problems in computational mechanics. The main difficulty that the spatial domain occupied by the fluid changes with time and the location of the boundary that depends on the fluid flow and the motion/deformation of the cable-stayed steel box girder bridge is usually an unknown. In this paper, a response analysis was carried out using ADINA (Automatic Dynamic Incremental Non-linear Analysis) to evaluate wind-induced dynamic response of the 3rd Jinan Yellow River Cable-stayed Bridge(ADINA corp.[2]). The bridge is semi-active separating from the bridge tower. Two ends of the steel box girder are connected with the bridge piers using spring connections.

2. Description of the 3rd Jinan Yellow River Cable-stayed Bridge and Numerical Model

The 3rd Jinan Yellow River Bridge[Fig1] [Fig 2] locates in Shandong Province of P. R. China. The full-length of the bridge is 4473.04m and the main bridge of it has four spans of 60+60+160+386m. Its deck of closed streamline cross-section of single box is 3.09 m high and 43.6m wide. The main girder of the cable-stayed bridge is divided into 46 segments which are streamlined flat steel box girders. According to different lengths and different thickness of the girders, there are seven styles of steel box girders in the main girder. The 3rd Jinan Yellow River cable-stayed bridge is semi-active separating from the bridge tower.

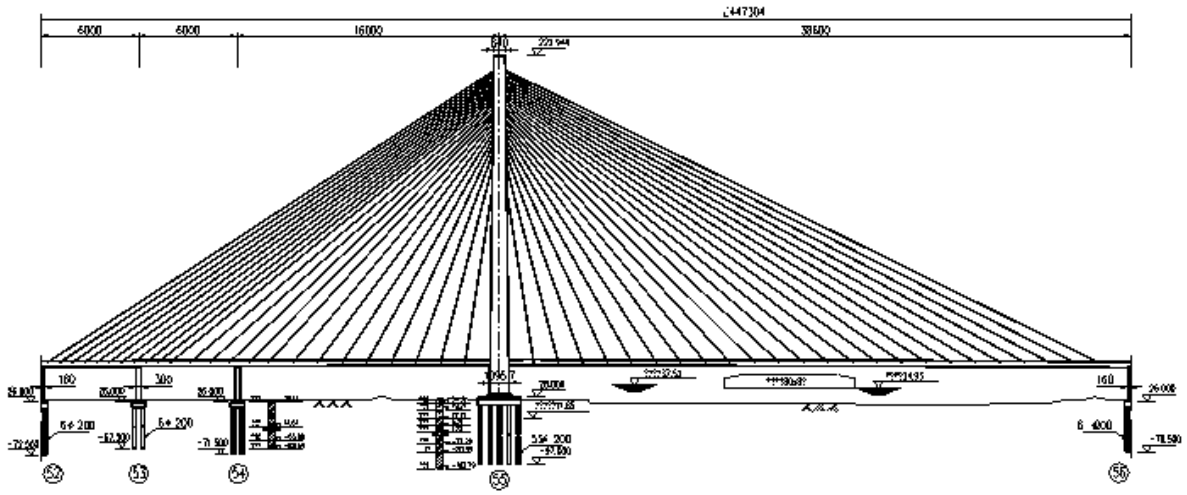

Figure 1: the front view of the bridge

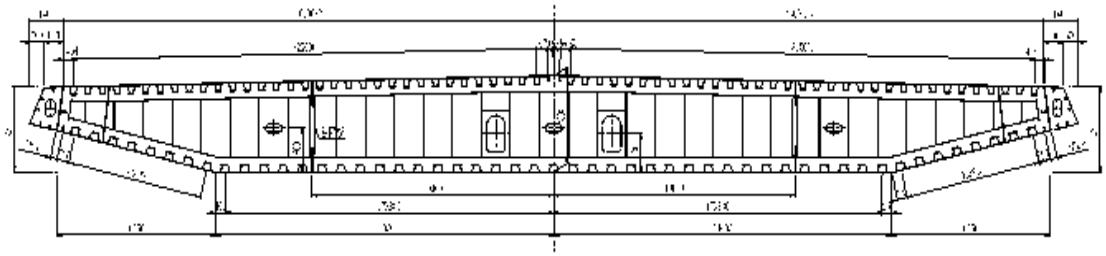

Figure 2: the cross section of the bridge

2.1 The structure model

The structure model[Fig3] is shown. The material of the steel box girders and inclined cables is elastic model whose elastic modulus E and Poisson's ration γ_1 are $2.06\times10^{11}N/m^2$ and 0.3 respectively, in addition to geometrical nonlinear effects such as large displacement in connection with small strain, isotropy-elastic material properties can be taken into account. In the finite element model, steel box girders are discretized by 4-node shell element in ADINA software. Meanwhile cables of the cable-stayed bridge are discretized by truss elements only subjected to tensile force in ADINA software. Two ends of the steel box girder are connected with the bridge piers using spring connections. The surfaces of the steel box girders and the corresponding fluid boundary are defined as the fluid-structure interface.

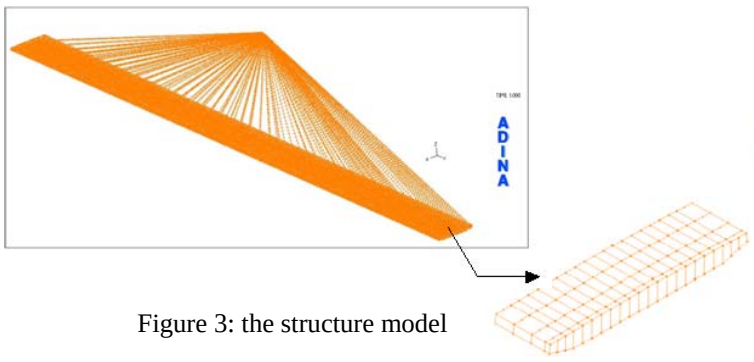

Figure 3: the structure model

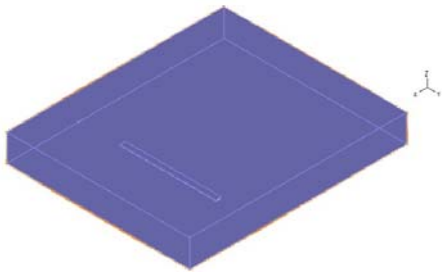

Figure 4: the fluid model

2.2 The fluid model

A full-scale model is introduced in numerical simulation. The dimension of the computational flow domain[Fig 4] is $1500m \times 1264.9m \times 187.28m$,and the windward of the steel box girders locates 479.59m away from the entrance and the leeward of the bridge locates 976.81m away from the outlet of the simulated wind tunnel. The fluid is modeled using the viscous and incompressible Navier-stokes equations with $k-\varepsilon$ turbulence model(K.J. Bathe[3]). The kinematical viscosity coefficient μ and air density ρ are $1.74\times10^{-5} kg/m \bullet s$ and $1.29 kg/m^3$ respectively. In this paper we used wind velocity profile to describe the distributed wind velocity at the inlet of flow. The formula is $\upsilon(z)=\left(\frac{z}{z_b}\right)^{\alpha}\upsilon_0$. The power law exponent α is 0.16. υ_0 represents the mean velocity at a height of $z_b=10m$ and it is 28.6m. The flow domain is discretized by 8 nodes hexahedron FCBI-C fluid element. The $x\times y\times z$ meshes used for fluid is $(45+2+8+8+2+8)\times(22+100+22)\times(3+1+22)$ with finer meshes near the structure.

2.3 The numerical simulation results

The fluid-structure analysis using ADINA-FSI is performed in the time domain until the response process shows a stationary condition. The results reveal the velocity in the flow domain, and typical features of the structure such as displacements, velocity and acceleration are obtained. Furthermore, the node displacement wind-induced dynamic coefficients are investigated. At last, the distributed wind pressure coefficient is calculated (Xinli Chen et al.[4]).

In Fig.5 the pressure band on the y=0 m cut section of the fluid domain is shown. The velocity behind the leeward is small. Fig.6 shows the x-velocity vector on the y=0m cut section near the section of the bridge deck. The time histories of every node's displacements, velocities and accelerations are also obtained.

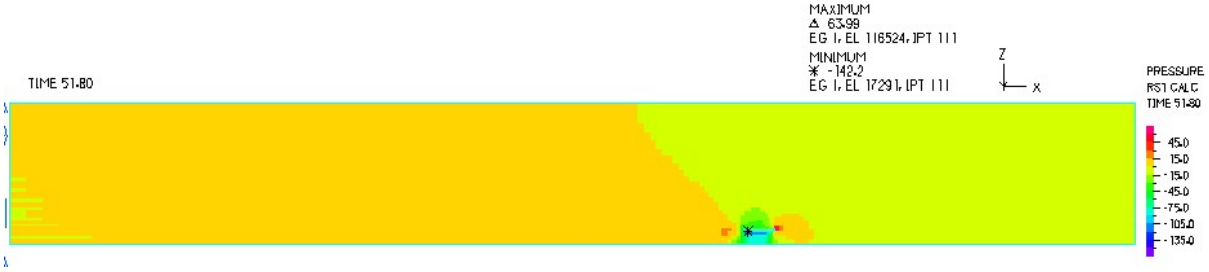

Figure 5: the pressure band on the y=0m cut section

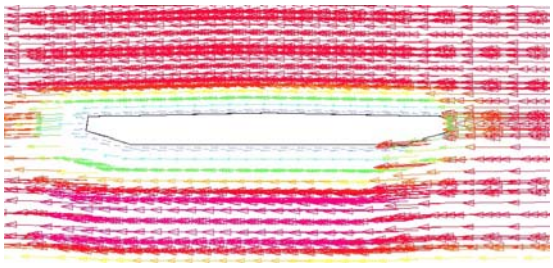

Figure 6: Details of the velocity band around the bridge deck

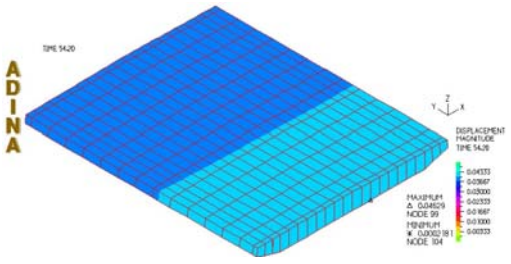

Figure 7: displacement of one end of the brdige

According to the results, the time-dependent displacement of every node is known, and from which the wind-induced dynamic coefficient can be calculated. So the wind-induced dynamic coefficients of windward surface and leeward surface of the 3rd Jinan Yellow River cable-stayed bridge are 1.52 and 1.55 respectively. Besides, the wind-induced dynamic coefficients of the top surface and the bottom surface of the bridge are 2.2 and 1.7.

The distributed pressure coefficient contour lines of some regions of the bridge are shown in Fig.7 and Fig.8.

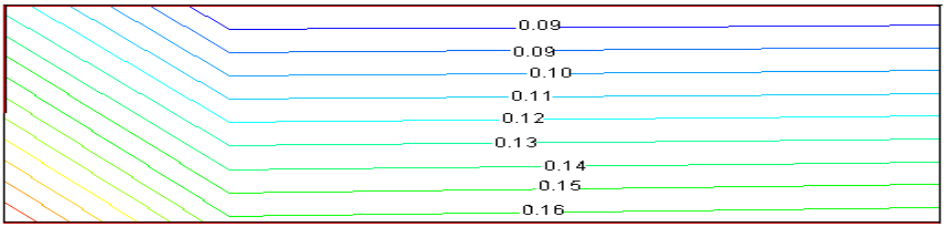

Figure 7: Distributed pressure coefficient contours of windward at the one end of the bridge

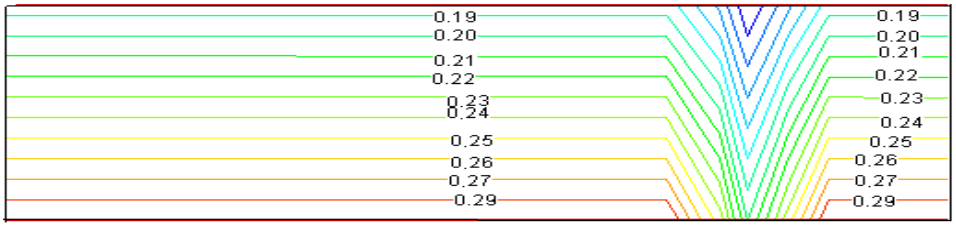

Figure 8: Distributed pressure coefficient contours of leedward in the middle of the bridge

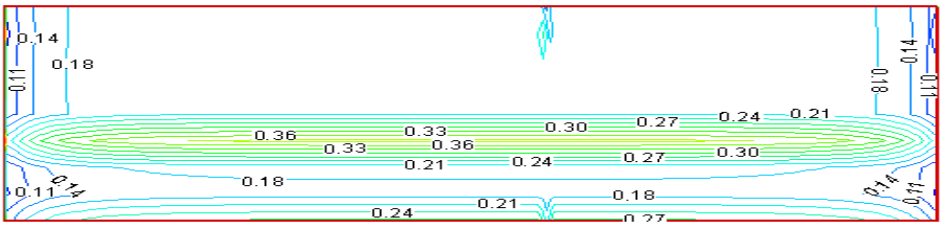

Figure 8: Distributed pressure coefficient contours of the bottom of the bridge

3. Conclusion

Three-dimensional ADINA simulations of the airflow around the 3rd Jinan Yellow River cable-stayed bridge were conducted to determine the pressure distributions on the sides of each surface and the distribution of the pressure differences. The velocity in the flow domain and typical features of the structure such as displacements and stresses are observed. Furthermore, the wind-induced dynamic coefficients and the wind pressure distribution coefficients are investigated.

References

[1] Zhengqing Chen. The Wind Engineering of the Bridge. China Communications Press, 2005.

[2] ADINA Theory and Modeling Guide Volume III□ADINA-F,Report ARD 04-09,2004.

[3] K.J. Bathe. Finite Element Procedures. Prentice-Hall, Inc., 1996

[4] Xinli Chen, Shizhao Shen, Yang Xiang.Wind-inducing Response Analysis and The Coefficient for Wind-Resistant Design of The Saddle-Shaped Membrane Structures. Journal of Tianjin Institute of Urban Construction 2001:7(3): 159-163.

[5] Dalin Tang, Chun Yang, David N. Ku, “A 3-D thin-wall model with fluid-structure interactions for blood flow in carotid arteries with symmetric and asymmetric stenoses”, Computers and Structures 72(1999) 357-377.

[6] Zhenhua Liu. Numerical Simulation of Fluid-Structure Interaction for Wind-induced Dynamic Response of Membrane Structures. Ph.D. Thesis. Department of Civil Engineering, Tongji University, 2006.

[7] G.K. Batchelor, An Introduction to Fluid Dynamics, Cambridge University Press,2000.

Proceedings of the 6th International Conference on
Computation of Shell and Spatial Structures
IASS-IACM 2008: "Spanning Nano to Mega"
28-31 May 2008, Cornell University, Ithaca, NY, USA
John F. ABEL and J. Robert COOKE (eds.)

A consistent finite element approximation for piezoelectric shell structures

Dieter LEGNER*, Sven KLINKEL, Werner WAGNER

*Institut für Baustatik, Universität Karlsruhe (TH)
Kaiserstr. 12, 76131 Karlsruhe, Germany
dieter.legner@bs.uni-karlsruhe.de

Abstract

In the field of technical applications piezoelectric sensors and actuators have typically a shell-like structure. A physical description leads to a system of electromechanical differential equations. For an approximative solution of the coupled boundary value problem the finite element method is employed. Therefore the classical shell formulation is extended by a piezoelectric part. The present shell element has four nodes and bilinear interpolation functions. The nodal degrees of freedom are displacements, rotations and the electric potential on top and bottom of the shell. In case of bending dominated problems incompatible approximation functions of the electrical and mechanical fields cause incorrect results. This effect occurs in standard element formulation, where the mechanical and electrical degrees of freedom are approximated with lowest order interpolation functions. In order to overcome this problem a mixed multi-field variational approach is introduced. It allows for approximations of the electric field and the strains independent of the bilinear interpolation functions. A quadratic approach for the shear strains and the corresponding electric field is proposed through the shell thickness. This leads to well balanced approximation functions regarding coupling of electrical and mechanical fields. A numerical example illustrates the more precise results in contrast to standard elements.

1. Introduction

Many papers on finite element models for the analysis of piezoelectric structures have appeared in the past, see e.g. Benjeddou [1] for a survey. Each formulation is especially apt to certain applications, but all of these only provide correct results when applied to cases of pure bending. However, this kind of load only rarely corresponds with reality. The present element is motivated by the desire to obtain correct results for bending dominated problems by means of the consistent approximation of the mechanical and electric fields.

2. Kinematics

The Green-Lagrangean strains $\mathbf{E}$ and shell strains $\boldsymbol{\varepsilon}_G$ derived from the kinematics according to Wagner and Gruttmann [4] are arranged in vectorial formation as follows:

$$\mathbf{E} = [E_{11},\, E_{22},\, E_{33},\, 2E_{12},\, 2E_{13},\, 2E_{23}]^T \quad , \quad \boldsymbol{\varepsilon}_G = [\overline{\varepsilon}_{11},\, \overline{\varepsilon}_{22},\, 2\overline{\varepsilon}_{12},\, \overline{\kappa}_{11},\, \overline{\kappa}_{22},\, 2\overline{\kappa}_{12},\, \overline{\gamma}_1,\, \overline{\gamma}_2]^T \quad . \tag{1}$$

Besides three degrees of freedom for the displacements $\mathbf{u}$ respectively rotations $\boldsymbol{\beta}$ we use two electrical degrees of freedom φ_o, φ_u to represent the electric potential on top and bottom of the shell structure. With

$$\varphi(\vartheta^1, \vartheta^2, \vartheta^3) = \frac{1}{t}[(\frac{t}{2} - \vartheta^3)\varphi_u(\vartheta^1, \vartheta^2) + (\frac{t}{2} + \vartheta^3)\varphi_o(\vartheta^1, \vartheta^2)] \quad , \quad \frac{t}{2} \leq \vartheta^3 \leq \frac{t}{2} \tag{2}$$

a linear approach is proposed for the electric potential through the thickness t, where ϑ^1, ϑ^2 are defined as in-plane co-ordinates and ϑ^3 as thickness co-ordinate of the shell. With $\vec{E}_i = -\frac{\partial \varphi}{\partial \xi^i}$ the components of the electric field are given as

$$\begin{aligned}
\vec{E_1} &= \left[\frac{1}{t}(\frac{t}{2}-\vartheta^3) \quad \frac{1}{t}(\frac{t}{2}+\vartheta^3)\right]\left[\begin{array}{c}\vec{\varepsilon_1}\\ \vec{\varepsilon_2}\end{array}\right] \quad , \\
\vec{E_2} &= \left[\frac{1}{t}(\frac{t}{2}-\vartheta^3) \quad \frac{1}{t}(\frac{t}{2}+\vartheta^3)\right]\left[\begin{array}{c}\vec{\varepsilon_3}\\ \vec{\varepsilon_4}\end{array}\right] \quad , \\
\vec{E_3} &= \left[\begin{array}{cc}\frac{1}{t} & -\frac{1}{t}\end{array}\right]\left[\begin{array}{c}\vec{\varepsilon_5}\\ \vec{\varepsilon_6}\end{array}\right] \quad .
\end{aligned} \tag{3}$$

Expanded by the corresponding piezoelectric components the continuum strains and shell strains finally read

$$\begin{aligned}
\left[\begin{array}{c}\mathbf{E}\\ \vec{\mathbf{E}}\end{array}\right] &= \left[E_{11},\, E_{22},\, E_{33},\, 2E_{12},\, 2E_{13},\, 2E_{23},\, \vec{E}_1,\, \vec{E}_2,\, \vec{E}_3\right]^T \quad , \\
\boldsymbol{\varepsilon}_G &= \left[\overline{\varepsilon}_{11},\, \overline{\varepsilon}_{22},\, 2\overline{\varepsilon}_{12},\, \overline{\kappa}_{11},\, \overline{\kappa}_{22},\, 2\overline{\kappa}_{12},\, \overline{\gamma}_1,\, \overline{\gamma}_2,\, \vec{\overline{\varepsilon}}_1,\, \vec{\overline{\varepsilon}}_2,\, \vec{\overline{\varepsilon}}_3,\, \vec{\overline{\varepsilon}}_4,\, \vec{\overline{\varepsilon}}_5,\, \vec{\overline{\varepsilon}}_6\right]^T \quad .
\end{aligned} \tag{4}$$

In order to set them in relation to each other a matrix $\mathbf{A}$ is introduced.

3. Constitutive equations

In accordance to a linear piezoelectric theory, see e.g. Maugin [3], the relations between stresses $\mathbf{S}$ and dielectric displacements $\vec{\mathbf{D}}$, strains $\mathbf{E}$ and the electric field $\vec{\mathbf{E}}$ are assumed to be

$$\left[\begin{array}{c}\mathbf{S}\\ -\vec{\mathbf{D}}\end{array}\right] = \left[\begin{array}{cc}\mathbb{C} & -\mathbb{e}^T\\ -\mathbb{e} & -\boldsymbol{\epsilon}\end{array}\right]\left[\begin{array}{c}\mathbf{E}\\ \vec{\mathbf{E}}\end{array}\right] \quad . \tag{5}$$

Herein $\mathbb{C}$ denotes the transversal isotropic elasticity matrix, $\mathbb{e}$ the piezoelectric matrix and in $\boldsymbol{\epsilon}$ the material permittivity is described. We define the stored energy function

$$W_0 = \frac{1}{2}\int_{(\Omega_0)} \boldsymbol{\varepsilon}^T \underbrace{\int_t \mathbf{A}^T \left[\begin{array}{cc}\mathbb{C} & -\mathbb{e}^T\\ -\mathbb{e} & -\boldsymbol{\epsilon}\end{array}\right]\mathbf{A}\, d\vartheta^3}_{\mathbb{D}}\, \boldsymbol{\varepsilon}\, dA \tag{6}$$

by using independent shell strains $\boldsymbol{\varepsilon}$

$$\left[\begin{array}{c}\boldsymbol{\varepsilon}_p\\ \boldsymbol{\varepsilon}_{33}\end{array}\right] = \left[\varepsilon_{11},\, \varepsilon_{22},\, 2\varepsilon_{12},\, \kappa_{11},\, \kappa_{22},\, 2\kappa_{12},\, \gamma_1,\, \gamma_2,\, \vec{\varepsilon}_1,\, \vec{\varepsilon}_2,\, \vec{\varepsilon}_3,\, \vec{\varepsilon}_4,\, \vec{\varepsilon}_5,\, \vec{\varepsilon}_6,\, \varepsilon^0_{33},\, \varepsilon^1_{33},\, \vec{\varepsilon}^{31}_{33},\, \vec{\varepsilon}^{22}_{33},\, \vec{\varepsilon}^{12}_{33}\right]^T \quad , \tag{7}$$

which are related to the expanded continuum strains by

$$\left[\begin{array}{c}\mathbf{E}\\ \vec{\mathbf{E}}\end{array}\right] = \underbrace{\left[\begin{array}{cccc}\mathbf{A}_1 & 0 & \mathbf{A}_2 & 0\\ 0 & \mathbf{A}_3 & 0 & \mathbf{A}_4\end{array}\right]}_{\mathbf{A}(\vartheta^3)}\underbrace{\left[\begin{array}{c}\boldsymbol{\varepsilon}_p\\ \boldsymbol{\varepsilon}_{33}\end{array}\right]}_{\boldsymbol{\varepsilon}(\vartheta^1,\,\vartheta^2)} \tag{8}$$

with

$$\mathbf{A}_1 = \left[\begin{array}{cccccccc}
1 & 0 & 0 & \vartheta^3 & 0 & 0 & 0 & 0\\
0 & 1 & 0 & 0 & \vartheta^3 & 0 & 0 & 0\\
0 & 0 & 0 & 0 & 0 & 0 & 0 & 0\\
0 & 0 & 1 & 0 & 0 & \vartheta^3 & 0 & 0\\
0 & 0 & 0 & 0 & 0 & 0 & q(\vartheta^3) & 0\\
0 & 0 & 0 & 0 & 0 & 0 & 0 & q(\vartheta^3)
\end{array}\right], \qquad \mathbf{A}_2 = \left[\begin{array}{cc}0 & 0\\ 0 & 0\\ 1 & \vartheta^3\\ 0 & 0\\ 0 & 0\\ 0 & 0\end{array}\right], \tag{9}$$

$$\mathbf{A}_3 = \left[\begin{array}{cccccc}
\frac{1}{t}(\frac{t}{2}-\vartheta^3) & 0 & \frac{1}{t}(\frac{t}{2}+\vartheta^3) & 0 & 0 & 0\\
0 & \frac{1}{t}(\frac{t}{2}-\vartheta^3) & 0 & \frac{1}{t}(\frac{t}{2}+\vartheta^3) & 0 & 0\\
0 & 0 & 0 & 0 & \frac{1}{t} & -\frac{1}{t}
\end{array}\right], \quad \mathbf{A}_4 = \left[\begin{array}{ccc}0 & 0 & q(\vartheta^3)\\ 0 & q(\vartheta^3) & 0\\ \vartheta^3 & 0 & 0\end{array}\right].$$

Herein a linear approach in thickness direction for both the strain and the electric field is used for the shell components $\boldsymbol{\varepsilon}_{33}$. Moreover, there is a quadratic approach, denoted by $q(\vartheta^3)$, for the shear components and the

electric fields in 1- and 2-direction across the thickness. According to the vectorial formation of the shell strain components we introduce the assumed shell stress resultants as

$$\tilde{\boldsymbol{\sigma}} = [\boldsymbol{\sigma},\, 0,\, 0,\, 0,\, 0,\, 0,\, 0]^T \;,\quad \boldsymbol{\sigma} = \left[n^{11},\, n^{22},\, n^{12},\, m^{11},\, m^{22},\, m^{12},\, q^1,\, q^2,\, \vec{d}_1,\, \vec{d}_2,\, \vec{d}_3,\, \vec{d}_4,\, \vec{d}_5,\, \vec{d}_6\right]^T \quad , \quad (10)$$

wherein all the components in thickness direction are enforced to be zero.

4. Variational formulation and finite element equations

Using a variational functional of the Hu-Washizu type, the weak form of the boundary value problem reads

$$\delta\Pi = \int\limits_{(\Omega_0)} [\delta\boldsymbol{\varepsilon}_G^T\boldsymbol{\sigma} + \boldsymbol{\sigma}^T(\boldsymbol{\varepsilon}_G - \boldsymbol{\varepsilon}_p) + \boldsymbol{\varepsilon}^T\,(\frac{\partial W_{0s}}{\partial\boldsymbol{\varepsilon}} - \tilde{\boldsymbol{\sigma}})]\; dA \;-\; \int\limits_{(\Omega_0)} \delta\mathbf{v}^T\overline{\mathbf{p}}\; dA \;-\; \int\limits_{(\partial\Omega_0)} \delta\mathbf{v}^T\overline{\mathbf{t}}\; ds \;= 0 \qquad (11)$$

with the body forces $\overline{\mathbf{p}}$, the traction vector $\overline{\mathbf{t}}$ and $\mathbf{v} = [u_1, u_2, u_3, \beta_1, \beta_2, \beta_3, \varphi_u, \varphi_o]^T$. For a solution we specify finite element equations considering a four node element. The displacements, rotations, electric potentials and the geometry are approximated with the same bilinear interpolation function

$$N_I(\xi,\eta) = \frac{1}{4}(1+\xi_I\xi)(1+\eta_I\eta) \quad , \quad \xi,\eta\;\epsilon\;[-1,1] \qquad (12)$$

at nodes $I = 1, 2, 3, 4$. With $\mathbf{v}_I = [u_1, u_2, u_3, \beta_1, \beta_2, \beta_3, \varphi_u, \varphi_o]_I^T$ we obtain

$$\mathbf{v}^h = \sum_{I=1}^{4}\mathbf{N}_I\mathbf{v}_I \quad , \quad \delta\mathbf{v}^h = \sum_{I=1}^{4}\mathbf{N}_I\delta\mathbf{v}_I \quad , \quad \boldsymbol{\varepsilon}_G^h = \sum_{I=1}^{4}\mathbf{B}_I\mathbf{v}_I \quad , \quad \delta\boldsymbol{\varepsilon}_G^h = \sum_{I=1}^{4}\mathbf{B}_I\delta\mathbf{v}_I \quad , \qquad (13)$$

wherein $\mathbf{B}_I$ contains the derivations of the shape functions. With independent variables in $\hat{\boldsymbol{\sigma}}$ and $\hat{\boldsymbol{\varepsilon}} = [\hat{\boldsymbol{\varepsilon}}_1, \hat{\boldsymbol{\varepsilon}}_2]^T$ the quantities of the assumed stress resultants $\boldsymbol{\sigma}^h$ and strains $\boldsymbol{\varepsilon}^h$ are given as

$$\boldsymbol{\sigma}^h = \mathbf{N}_\sigma\hat{\boldsymbol{\sigma}} \quad , \quad \boldsymbol{\varepsilon}^h = \mathbf{N}_\varepsilon\hat{\boldsymbol{\varepsilon}} \quad , \quad \mathbf{N}_\varepsilon = \left[\mathbf{N}_\varepsilon^1, \mathbf{N}_\varepsilon^2\right] \qquad (14)$$

with

$$\mathbf{N}_\sigma = \begin{bmatrix} \mathbf{1}_3 & \mathbf{0} & \mathbf{0} & \mathbf{N}_\sigma^m & \mathbf{0} & \mathbf{0} & \mathbf{0} \\ \mathbf{0} & \mathbf{1}_3 & \mathbf{0} & \mathbf{0} & \mathbf{N}_\sigma^b & \mathbf{0} & \mathbf{0} \\ \mathbf{0} & \mathbf{0} & \mathbf{1}_2 & \mathbf{0} & \mathbf{0} & \mathbf{N}_\sigma^s & \mathbf{0} \\ \mathbf{0} & \mathbf{0} & \mathbf{0} & \mathbf{0} & \mathbf{0} & \mathbf{0} & \mathbf{N}_{\vec{d}} \end{bmatrix} \;,\; \mathbf{N}_{\vec{d}} = \begin{bmatrix} \mathbf{1}_2 & \mathbf{0} & \mathbf{0} & \mathbf{N}_{\vec{d}}^u & \mathbf{0} & \mathbf{0} \\ \mathbf{0} & \mathbf{1}_2 & \mathbf{0} & \mathbf{0} & \mathbf{N}_{\vec{d}}^o & \mathbf{0} \\ \mathbf{0} & \mathbf{0} & \mathbf{1}_2 & \mathbf{0} & \mathbf{0} & \mathbf{N}_{\vec{d}}^h \end{bmatrix} \;, \qquad (15)$$

$$\mathbf{N}_{\vec{d}}^u = \mathbf{N}_{\vec{d}}^o = \mathbf{J}^{0^T}\begin{bmatrix} \xi^2 & 0 \\ 0 & \xi^1 \end{bmatrix} \;,\; \mathbf{N}_{\vec{d}}^h = \begin{bmatrix} \xi^1 & \xi^2 & \xi^1\xi^2 & 0 & 0 & 0 \\ 0 & 0 & 0 & \xi^1 & \xi^2 & \xi^1\xi^2 \end{bmatrix}$$

and

$$\mathbf{N}_\varepsilon^1 = \begin{bmatrix} \mathbf{1}_3 & \mathbf{0} & \mathbf{0} & \mathbf{N}_\varepsilon^{m1} & \mathbf{0} & \mathbf{0} & \mathbf{0} \\ \mathbf{0} & \mathbf{1}_3 & \mathbf{0} & \mathbf{0} & \mathbf{N}_\varepsilon^{b1} & \mathbf{0} & \mathbf{0} \\ \mathbf{0} & \mathbf{0} & \mathbf{1}_2 & \mathbf{0} & \mathbf{0} & \mathbf{N}_\varepsilon^{s1} & \mathbf{0} \\ \mathbf{0} & \mathbf{0} & \mathbf{0} & \mathbf{0} & \mathbf{0} & \mathbf{0} & \mathbf{N}_{\vec{\varepsilon}} \\ \mathbf{0} & \mathbf{0} & \mathbf{0} & \mathbf{0} & \mathbf{0} & \mathbf{0} & \mathbf{0} \\ \mathbf{0} & \mathbf{0} & \mathbf{0} & \mathbf{0} & \mathbf{0} & \mathbf{0} & \mathbf{0} \\ \mathbf{0} & \mathbf{0} & \mathbf{0} & \mathbf{0} & \mathbf{0} & \mathbf{0} & \mathbf{0} \\ \mathbf{0} & \mathbf{0} & \mathbf{0} & \mathbf{0} & \mathbf{0} & \mathbf{0} & \mathbf{0} \end{bmatrix} \;,\; \mathbf{N}_\varepsilon^2 = \begin{bmatrix} \mathbf{0} & \mathbf{N}_\varepsilon^{m2} & \mathbf{0} & \mathbf{0} & \mathbf{0} & \mathbf{0} \\ \mathbf{0} & \mathbf{0} & \mathbf{N}_\varepsilon^{b2} & \mathbf{0} & \mathbf{0} & \mathbf{0} \\ \mathbf{0} & \mathbf{0} & \mathbf{0} & \mathbf{0} & \mathbf{0} & \mathbf{0} \\ \mathbf{0} & \mathbf{0} & \mathbf{0} & \mathbf{0} & \mathbf{0} & \mathbf{0} \\ \mathbf{N}_\varepsilon^{z2} & \mathbf{0} & \mathbf{0} & \mathbf{0} & \mathbf{0} & \mathbf{0} \\ \mathbf{0} & \mathbf{0} & \mathbf{0} & \mathbf{N}_{\vec{\varepsilon}_3}^{z2} & \mathbf{0} & \mathbf{0} \\ \mathbf{0} & \mathbf{0} & \mathbf{0} & \mathbf{0} & \mathbf{N}_{\vec{\varepsilon}_2}^{z2} & \mathbf{0} \\ \mathbf{0} & \mathbf{0} & \mathbf{0} & \mathbf{0} & \mathbf{0} & \mathbf{N}_{\vec{\varepsilon}_1}^{z2} \end{bmatrix} \;,$$

$$\mathbf{N}_{\vec{\varepsilon}} = \mathbf{N}_{\vec{d}} \quad , \quad \mathbf{N}_{\vec{\varepsilon}_1}^{z2} = [1] \quad , \quad \mathbf{N}_{\vec{\varepsilon}_2}^{z2} = [1] \quad , \quad \mathbf{N}_{\vec{\varepsilon}_3}^{z2} = [1] \quad . \qquad (16)$$

For the definitions of $\mathbf{N}_\sigma^m$, $\mathbf{N}_\sigma^b$, $\mathbf{N}_\sigma^s$, $\mathbf{N}_\varepsilon^{m1}$, $\mathbf{N}_\varepsilon^{b1}$, $\mathbf{N}_\varepsilon^{s1}$, $\mathbf{N}_\varepsilon^{z2}$, $\mathbf{N}_\varepsilon^{m2}$ and $\mathbf{N}_\varepsilon^{b2}$ see Klinkel *et al.* [2]. Thus, with

$$\mathbf{H} = \int\limits_{(\Omega_e)} \mathbf{N}_\varepsilon^T\,\mathbb{D}\,\mathbf{N}_\varepsilon\, dA \quad , \quad \mathbf{F} = \int\limits_{(\Omega_e)} \mathbf{N}_\varepsilon^T\,\tilde{\mathbf{N}}_\sigma\, dA \quad , \quad \mathbf{G} = \int\limits_{(\Omega_e)} \mathbf{N}_\sigma^T\,\mathbf{B}\, dA \qquad (17)$$

we obtain the following approximation on element level

$$\delta^h \Pi = \sum_{e=1}^{numel} \begin{bmatrix} \delta\mathbf{v} \\ \delta\hat{\boldsymbol{\varepsilon}} \\ \delta\hat{\boldsymbol{\sigma}} \end{bmatrix}_e^T \left(\begin{bmatrix} \mathbf{0} & \mathbf{0} & \mathbf{G}^T \\ \mathbf{0} & \mathbf{H} & -\mathbf{F} \\ \mathbf{G} & -\mathbf{F}^T & \mathbf{0} \end{bmatrix} \begin{bmatrix} \mathbf{v} \\ \hat{\boldsymbol{\varepsilon}} \\ \hat{\boldsymbol{\sigma}} \end{bmatrix} - \begin{bmatrix} \mathbf{f_a} \\ \mathbf{0} \\ \mathbf{0} \end{bmatrix} \right) = 0 \quad . \tag{18}$$

Considering that the finite element interpolations for the fields $\boldsymbol{\varepsilon}$ and $\tilde{\boldsymbol{\sigma}}$ are discontinuous across the element boundaries, $\hat{\boldsymbol{\varepsilon}}$ and $\hat{\boldsymbol{\sigma}}$ can be condensed on element level and we obtain the element stiffness matrix $\mathbf{k}_T^e$ as

$$\sum_{e=1}^{numel} \delta\mathbf{v}^T (\underbrace{\mathbf{G}^T \left[\mathbf{F}^T \mathbf{H}^{-1} \mathbf{F}\right]^{-1} \mathbf{G}}_{\mathbf{k}_T^e} \mathbf{v} - \mathbf{f}_a) = 0 \quad . \tag{19}$$

5. Example

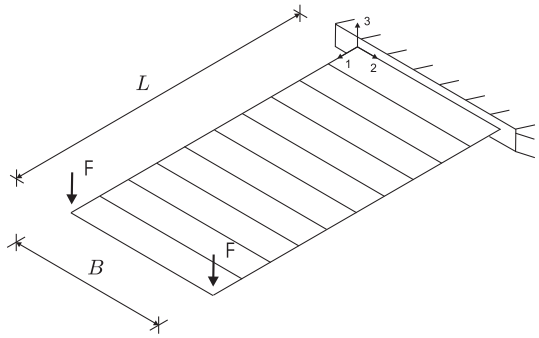

Geometry data:
$t = 0.01\,m\,,\ L = 0.24\,m\,,\ B = 0.12\,m$
Material properties:
$E_1 = E_2 = E_3 = 123 \cdot 10^9\ N/m^2$
$G_{12} = G_{13} = G_{23} = 61.5 \cdot 10^9\ N/m^2$
$\mathbb{e}_{13} = -5\,C/m^2\,,\ \epsilon = 12.5 \cdot 10^{-9}\,C/Nm^2$
electric boundary condition:
$\varphi_u = 0\,V$
nodal force:
$F = 4.17\,kN$

Figure 1: Finite element mesh with geometry and material data, load and boundary conditions

With the concept proposed the numerical solution of this bending dominated problem reads for the displacement $u_{max} = 3.067 \cdot 10^{-2}\,m$ and for the electric potential at the upper side $\varphi_o \approx 0\,V$. The results are very close to the analytical solution ($u_{max} = 3.068 \cdot 10^{-2}\,m$, $\varphi_o = 0\,V$). Using standard element formulation without internal degrees of freedom we are too kept from finding the analytical solution ($u_{max} = 3.117 \cdot 10^{-2}\,m$, $\varphi_o = 1.055 \cdot 10^4\,V$).

6. Conclusion

The given example already shows the advantages of well balanced approximation functions regarding coupling of electrical and mechanical fields. This is of particular importance for more complicated shell applications in the analysis of piezoelectric structures.

Acknowledgement

The financial support of the Deutsche Forschungsgemeinschaft for the first author is acknowledged gratefully.

References

[1] Benjeddou A. Advances in piezolelectric finite element modeling of adaptive structural elements: a survey. *Computers and Structures* 2000 ; **76**:347-363.

[2] Klinkel S, Gruttmann F, Wagner W. A mixed shell formulation accounting for thickness strains and finite strain 3d-material models. *International Journal for Numerical Methods in Engineering* 2007; in press.

[3] Maugin GA. Continuum mechanics of electromagnetic solids. In *Applied Mathematics and Mechanics*, Achenbach JD, Budiansky B, Koiter WT, Lauwerier HA, Van Wijngaarden L (eds). North-Holland Series: Amsterdam, 1988 ; **33**.

[4] Wagner W and Gruttmann F. A robust non-linear mixed hybrid quadrilateral shell element. *International Journal for Numerical Methods in Engineering* 2005 ; **64**:635-666.

Proceedings of the 6th International Conference on
Computation of Shell and Spatial Structures
IASS-IACM 2008: "Spanning Nano to Mega"
28-31 May 2008, Cornell University, Ithaca, NY, USA
John F. ABEL and J. Robert COOKE (eds.)

Vibration Analysis of Thin-Walled - Gas or Fluid Filled - Structures Including the Effect of the Inflation/Filling Process

Karl Schweizerhof*, Marc Haßler

Institut für Mechanik, Universität Karlsruhe (TH)
Englerstr. 2, D-76131 Karlsruhe, Germany
karl.schweizerhof@ifm.uni-karlsruhe.de

Abstract

Fluid-structure interaction problems involving thin-walled membrane and shell-type structures undergoing large deformations can be considered in a step-wise fashion. Using conventional finite elements [1],[6],[8] for the discretization of the fluid or gas domain leads to heavily distorted meshes for the fluid if e.g. inflation or filling processes including large deformations are to be investigated. Although with ALE based algorithms this problem can be solved by a permanent remeshing of the fluid domain parts in the vicinity of the structural mesh, this is at the expense of high computational effort. Benefitting from an algorithm, which replaces the fluid or gas filling by an energetically equivalent volume dependent surface loading (see e.g. [2]-[5] and [7]) such primarily static inflation processes can be simulated without discretizing the fluid or gas domain. Thus the deformation dependent inner state variables of the fluid or gas can be computed avoiding the previously mentioned difficulties with mesh distortions in an efficient way. In a following step the fluid parameters such as fluid level and information about the wetted structural parts can then be used to define properly the initial conditions for a dynamic finite element analysis of gas or fluid filled structures while using standard acoustic finite elements to compute e.g. vibration modes.

1 Virtual Work Approach of Gas or Fluid Loaded Structures

For a state of equilibrium in a system consisting of a fluid domain $\mathcal{F}$ and a solid domain $\mathcal{B}$ the variation $\delta\mathcal{E}$ of the total energy has to fulfill

$$\delta\mathcal{E} = \delta\mathcal{E}^{\mathcal{B}} + \delta\mathcal{E}^{\mathcal{F}} = 0 \ . \tag{1}$$

Assuming an adiabatic system, without any heat change $\delta\mathcal{Q}$, the energy conservation in the fluid and solid domain only consists of the variations $\delta\mathcal{T}^{\mathcal{B}\cup\mathcal{F}}$ and $\delta\mathcal{U}^{\mathcal{B}\cup\mathcal{F}}$ of the kinetic and the internal energy and of the virtual work $\delta\mathcal{W}^{\mathcal{B}\cup\mathcal{F}}$ of the external forces.

$$\delta\mathcal{E} = \delta\mathcal{T}^{\mathcal{B}\cup\mathcal{F}} + \delta\mathcal{U}^{\mathcal{B}\cup\mathcal{F}} - \delta\mathcal{W}^{\mathcal{B}\cup\mathcal{F}} = 0 \tag{2}$$

Introducing the virtual displacement field $\delta\boldsymbol{u}$, the accelerations $\ddot{\boldsymbol{u}}$ and the density ρ, the variation of the total kinetic energy can be written as

$$\delta\mathcal{T}^{\mathcal{B}\cup\mathcal{F}} = \int\limits_{\mathcal{B}\cup\mathcal{F}} \rho\ddot{\boldsymbol{u}} \cdot \delta\boldsymbol{u} \ dv \ . \tag{3}$$

The stress tensor $\boldsymbol{\sigma}$ and the virtual strains $\boldsymbol{\varepsilon}$ lead to the variation of the internal energy:

$$\delta\mathcal{U}^{\mathcal{B}\cup\mathcal{F}} = \int\limits_{\mathcal{B}\cup\mathcal{F}} \boldsymbol{\sigma} : \delta\boldsymbol{\varepsilon} dv \ . \tag{4}$$

Hence, the weak form (2) can be used for a finite element formulation to describe the fluid-structure interaction. The fact that inflation processes usually imply large deformations, which would lead to a high computational effort, if the fluid was disctretized with finite elements, in the following section an alternative way is briefly presented, using an analytical meshfree description of the fluid domain.

1.1 Quasi static inflation

The goal of the approach [3] is to replace the fluid by an energetically equivalent surface load, assuming that the fluid can be understood as a one-phase system, which means it is fully described by its inner state variables as e.g. pressure p or density ρ. As the detailed derivation for an arbitrary combination of gas and/or fluid loaded shell structures can be found in [3] this section contains only the basic idea of the algorithm for the example of a pneumatic single degree of freedom system. For the general case the finite element set of equations is of the same structure. However, considering the fluid as a one-phase system with only a few degrees of freedom simulations are limited to quasi static processes, because no information of acoustic wave propagation inside the fluid can be provided. For the quasi static case the variation of the kinetic energy can be neglected in the energy conservation (2).

$$\delta\mathcal{T}^{\mathcal{F}} = 0 \tag{5}$$

The fact that the fluid is a one-phase system can also be used to simplify the stress tensor to

$$\boldsymbol{\sigma} = -p\boldsymbol{I} \ , \tag{6}$$

with $\boldsymbol{I}$ as the unit tensor. After integrating over the fluid volume $\mathcal{F}$ and using

$$\boldsymbol{I} : \delta\boldsymbol{\varepsilon} = \mathrm{trace}(\delta\boldsymbol{\varepsilon}) = \delta v / v \tag{7}$$

the variation of internal energy of the fluid domain can be given as

$$\delta\mathcal{U}^{\mathcal{F}} = -p\delta v \tag{8}$$

and thus the total variation $\delta\mathcal{E}^{\mathcal{F}}$ of the potential energy of the fluid yields

$$\delta\mathcal{E}^{\mathcal{F}} = -p\delta v - \delta\mathcal{W}^{\mathcal{F}} \ . \tag{9}$$

1.1.1 1D example

We consider a closed system with rigid walls and one single degree of freedom u as depicted in figure 1. The elastic solid domain is represented by the spring with stiffness k and the fluid domain consists of an enclosed gas volume v with a pressure p. The system is subjected to an external force f^{ext}. For a state of equilibrium equation (2) yields with (5)

$$\delta\mathcal{E} = ku\delta u - p\delta v - f^{ext}\delta u = 0 \ . \tag{10}$$

For a given cross section A of the moving rigid wall the virtual volume change δv can be written in terms of the virtual displacement δu.

$$\delta v = A\delta u \tag{11}$$

Linearization of the equilibrium condition (10) at a current state t within a Newton scheme leads to

$$\delta\mathcal{E}_{lin} = (ku_t - p_t A - f^{ext})\delta u + k\Delta u\delta u + \Delta pA\delta u = 0 \ . \tag{12}$$

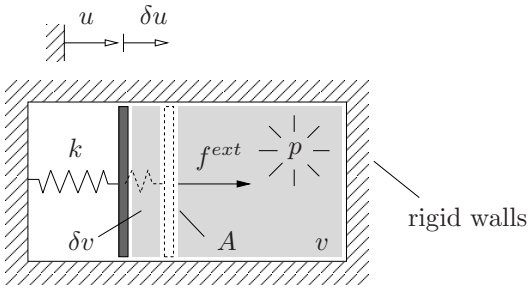

Figure 1: Virtual displacement δu applied to a pneumatic system with one degree of freedom u

Assuming isothermal behavior of the gas Boyle's law with $pv = const$ results in an equation for the incremental pressure change Δp, needed in equation (12):

$$\Delta p = -\frac{p_t}{v_t}\Delta v = -\frac{p_t}{v_t}A\Delta u \ . \tag{13}$$

Using equation (13) in (12) yields a fully displacement dependent formulation for the linearized state of equilibrium t with $u_{t+1} = u_t + \Delta u$.

$$\delta\mathcal{E}_{lin} = (ku_t - p_t A - f^{ext})\delta u + k\Delta u\delta u + \frac{p_t}{v_t}AA\Delta u\delta u = 0 \tag{14}$$

Eliminating the virtual displacement δu finally leads, along with the vector of the internal and external forces

$$f = f^{ext} - ku_t + p_t A \ , \tag{15}$$

to the equation for the unknown incremental displacement Δu.

$$\left(k + \frac{p_t}{v_t}AA\right)\Delta u = f \tag{16}$$

It can be seen that the volume dependence of the gas loading has both an influence on the stiffness and on the loading of the system. As already mentioned the general finite element formulation of a gas loaded shell structure (see e.g. [2], [4]) basically shows the same structure as equation (16) now with $\Delta\underline{d}$ as the nodal displacement vector: The stiffness matrix $\underline{K}$ is updated by a dyadic product of the discrete area vector $\underline{a}$ and the nodal force vector $\underline{f}$ is updated by the current pressure p_t.

$$\left(\underline{K} + \frac{p_t}{v_t}\underline{a}\underline{a}^T\right)\Delta\underline{d} = \underline{f} \tag{17}$$

For any arbitrary combination of fluid and/or gas loadings see [3].

1.2 Acoustic Fluid-Structure Interaction

After benefitting from the meshless but quasi static description of the fluid, the results obtained in the preceeding computation can serve as initial conditions in a subsequent dynamic analysis of the inflated and prestressed structure. Because in the vibration analysis the fluid mesh does not suffer from heavy distortions, it can be easily meshed with standard displacement dependent fluid elements, see e.g. [8] or [1], now allowing for kinetic energy changes (3). Discretizing both the position vector $\underline{X}_e$ and the displacement vector $\underline{u}_e$ of the fluid finite element with isoparametric shape functions $\underline{N}$, such that

$$\underline{X}_e = \underline{N}\hat{\underline{X}}_e \quad \text{and} \quad \underline{u}_e = \underline{N}\underline{d}_e \tag{18}$$

(with $\underline{\hat{X}}_e$ denoting the discrete nodal coordinates and $\underline{d}_e$ denoting the discrete nodal displacements), the kinematics resp. the volume changes of the element can be described. Introducing the matrix $\underline{B}$, the virtual and incremental volume changes on element level can be given as

$$\delta v = \int_{\mathcal{F}} \underline{B} \delta \underline{d}_e dv \quad \text{and} \quad \Delta v = \int_{\mathcal{F}} \underline{B} \Delta \underline{d}_e dv \tag{19}$$

and thus also the incremental pressure change

$$\Delta p = - \int_{\mathcal{F}} \frac{p_t}{v_t} \underline{B}_t \Delta \underline{d}_e dv \ , \tag{20}$$

necessary for the linearized weak form. Finally the linearized weak form of equilibrium at a current state t for a fluid element used for the subsequent vibration analysis follows as

$$\delta \mathcal{E}^{\mathcal{F}}_{lin} = \delta \mathcal{E}^{\mathcal{F}}_t + \delta \underline{d}_e{}^T \int_{\Omega_e} \rho_t \underline{N}^T \underline{N} dv \ \Delta \ddot{\underline{d}}_e + \delta \underline{d}_e^T \int_{\Omega_e} \frac{p_t}{v_t} \underline{B}^T \underline{B} dv \ \Delta \underline{d}_e - \delta \mathcal{W}^{\mathcal{F}} \ . \tag{21}$$

The third term in equation (21) is the analogon to the rank update in equation (17), with the difference that in (17) the energy of the fluid is described via the surrounding wetted surface $\partial \mathcal{B}$ of the solid domain and not by the volume integral over fluid elements as done in (21). Now an eigenvalue analysis is performed to find the eigenfrequencies and eigenmodes of the fluid filled an already highly deformed structure incorporating prestressing of the surrounding shell/membrane structure.

References

[1] Belytschko TB and Kennedy JM. A fluid-structure finite element method for the analysis of reactor safety problems. *Nuclear Engineering and Design* 1976; **38**:71–81.

[2] Bonet J, Wood RD, Mahaney J and Heywood P. Finite element analysis of air supported membrane structures. *Computer Methods in Applied Mechanics and Engineering* 2000; **190**:579–595.

[3] Haßler M and Schweizerhof K. On the static interaction of fluid and gas loaded multi-chamber systems in large deformation finite element analysis. *Computer Methods in Applied Mechanics and Engineering* 2008; **197**:1725–1749.

[4] Rumpel T and Schweizerhof K. Volume-dependent pressure loading and its influence on the stability of structures. *International Journal for Numerical Methods in Engineering* 2003; **56**:211–238.

[5] Rumpel T and Schweizerhof K. Hydrostatic Fluid Loading in Non-Linear Finite Element Analysis. *International Journal for Numerical Methods in Engineering* 2004; **59**:849–870.

[6] Schotte JS and Ohayon R. Effect of gravity on a free-free elastic tank partially filled with incompressible liquid. *Journal of Fluids and Structures* 2003; **18**:215–226.

[7] Schweizerhof K and Ramm E. Displacement Dependent Pressure Loads in Nonlinear Finite Element Analyses. *Computers & Structures* 1984; **18**:1099–1114.

[8] Wang X and Bathe KJ. Displacement/pressure based mixed finite element formulations for acoustic fluid-structure interaction problems. *International Journal for Numerical Methods in Engineering* 1997; **40**:2001–2017.

Proceedings of the 6th International Conference on
Computation of Shell and Spatial Structures
IASS-IACM 2008: "Spanning Nano to Mega"
28-31 May 2008, Cornell University, Ithaca, NY, USA
John F. ABEL and J. Robert COOKE (eds.)

Thin-walled Structures Interacting with Incompressible Flows

Ekkehard RAMM*, Malte VON SCHEVEN, Christiane FÖRSTER, Wolfgang A. WALL

* Institut für Baustatik und Baudynamik, Universität Stuttgart
Pfaffenwaldring 7, 70550 Stuttgart, Germany
ramm@ibb.uni-stuttgart.de

Formulation

The interaction of incompressible flows and thin-walled structures such as membranes and shells is a particular challenge because both partners are physically extremely sensitive. The response of slender structures may very much depend on slight changes of initial parameters; for example geometrical imperfections may drastically reduce the buckling load of thin shell. A similar situation exists for flow problems where the incompressibility plays a dominant role. It is obvious that this delicate behavior carries over if thin-walled structures with low mass interact with an incompressible flow. This sensitivity in turn reflects on the numerical solution procedure, in other words each numerical scheme supposedly robust for the individual constituent might deteriorate for the coupled problem. The contribution presents a partitioned fluid-structure interaction algorithm based on a second order accurate structural solver employing solid shell elements and an Arbitrary Lagrangean Eulerian flow formulation.

The shell model includes geometrical nonlinearities and allows for the use of fully three dimensional material laws without modification [1]. This seven-parameter shell formulation is depicted in Fig. 1. In addition to the classical Reissner-Mindlin kinematics (yielding five degrees of freedom per node) it contains the thickness stretch leading to an additional degree of freedom and a seventh strain degree of freedom which allows for a linearly varying strain E_{33} in shell thickness direction.

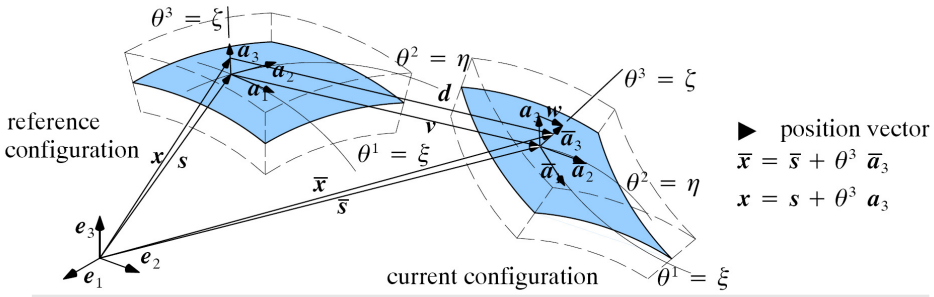

Figure 1: Seven parameter shell formulation.

This strain degree of freedom is locally introduced by means of the enhanced assumed strain method (EAS) and condensed out on element base prior to assembly. This formulation is asymptotically correct and the lowest

possible approach which allows a complete three-dimensional description. The temporal discretization of is performed by means of the generalized-α time discretization.

The Newtonian fluid is governed by the incompressible Navier-Stokes equations formulated in a deforming ALE frame of reference. One-step-θ time integration and second order backward differentiation (BDF2) are used for temporal discretization. As spatial discretization stabilized equal order finite elements are used. Pseudo structural mesh motion schemes are applied where the mesh domain is treated as a continuum.

Selected aspects of the individual constituents and their interaction are discussed; among them are the problem of conditioning for the shell model, the flow solver satisfying the geometric conservation law and the reliability of the fluid formulation in case of small time steps and distorted mesh [2].

It is well-known that sequential coupling approaches, often used for their computational efficiency, may fail in certain situations when the incompressible flow interacts with an extremely slender low mass structure. It can be shown by a rigorous analysis that this is due to the so-called artificial added mass effect [3] being an inherent instability that unfortunately cannot be removed by reducing the time steps size. As a remedy a strongly coupled partitioning algorithm is applied iteratively adjusting the interface conditions; here different dynamically adapted relaxation methods can be utilized to accelerate the convergence of the iteration. Further details are given in [4] and [5].

The following two numerical examples demonstrate the capabilities of the formulation.

Flow in a Collapsible Tube

This example describes the problem of viscous flow in an elastic tube. Elastic tubes collapse, i.e. buckle non-axisymmetrically when the transmural pressure (internal minus external pressure) falls below a critical value. The tube's large deformation during the buckling causes a strong interaction between fluid and solid. To illustrate the response of the tube we consider its deformation in a procedure in which the flow rate is prescribed by means of a volumetric pump attached to the upstream end of the tube, see Fig. 2.

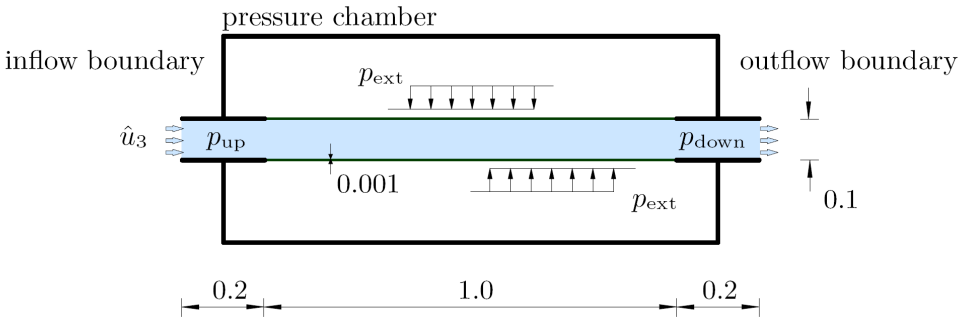

Figure 2: Problem definition collapsing tube.

The material of the tube has a Young's modulus of $E = 8.75 * 10^8$ N/cm^2, Poisson's ratio of $\nu^S = 0.3$ and a mass density of $\rho^S = 7.5$ g/cm^3. The tube is passed by water with a density of $\rho^F = 1.0$ g/cm^3, a kinematic viscosity of $\nu^F = 0.01$ cm^2/s and the prescribed inflow velocity is $\hat{u}_3 = 1.0$ cm/s.

We keep the fluid pressure at the far downstream end of the tube constant, $p_{down} = 0.0$, and induce its collapse by increasing the chamber pressure. As the chamber pressure is increased, the transmural pressure decreases and first becomes negative (compressive) at the downstream end. When the compressive load exceeds a critical value, the axisymmetric deformation loses its stability and the tube buckles non-axisymmetrically. Figure 3 shows the wall deformation of the tube as the non-axisymmetric collapse progresses.

Basin with Collapsing Arch

This example involves a two-dimensional basin as depicted in Fig. 4. It demonstrates the capability of the generalized free surface description in our FSI solver. The lateral walls and parts of the bottom are rigid. The center part of the bottom is closed by an elastic arch. The initial fluid depth is 20.0 cm. The basin is filled through two lateral channels with $\hat{u}_2 = 5.0$ cm/s.

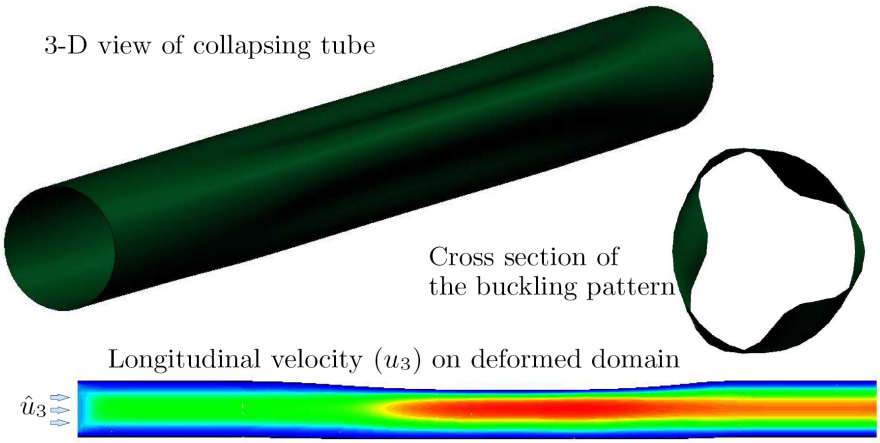

Figure 3: Tube deformation.

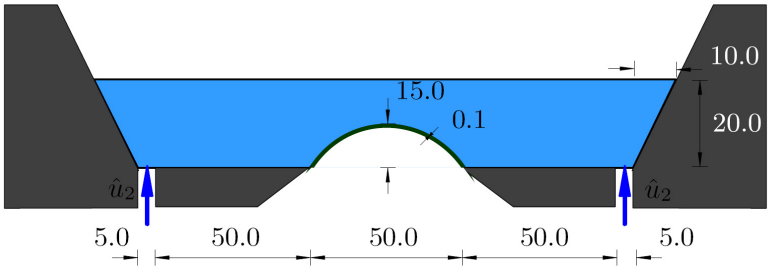

Figure 4: Basin with elastic arch: initial configuration.

The elastic arch has a thickness of 0.1 cm. The structural material parameters were chosen to $\rho^S = 500$ g/cm^3, $E = 9.0 * 10^8$ N/cm^2 and $\nu^S = 0.3$. The fluid density is $\rho^F = 1.0$ g/cm^3 and the kinematic viscosity is $\nu^F = 9.0$ cm^2/s. At both lateral inclined walls slip boundary conditions were applied. The fluid domain was discretized with 3200 Q1Q1 stabilized fluid elements. The time increment was chosen to $\Delta t = 0.025$ s.

Due to the increasing fluid height the pressure on the elastic arch reaches a critical value and the structure collapses. As shown in Fig. 5, the present approach is able to reproduce this highly transient coupled buckling process exhibiting large structural and free surface deformations. Due to the damping of the fluid the system reaches a new steady equilibrium position after approximately t = 72.0 s.

References

[1] M. Bischoff and E. Ramm: On the physical significance of higher order kinematic and static variables in a three-dimensional shell formulation. *International Journal for Solids and Structures*, 37 (2000), 6933-6960.

[2] Ch. Förster, W.A. Wall and E. Ramm: On the geometric conservation law in transient flow calculations on deforming domains. *International Journal for Numerical Methods in Fluids*, 50 (2006), 1369-1379.

[3] Ch. Förster, W.A. Wall and E. Ramm: Artificial added mass instabilities in sequential staggered coupling of nonlinear structures and incompressible flow. *Computer Methods in Applied Mechanics and Engineering*, 196 (2007), 1278-1293.

[4] W. A. Wall, A. Gerstenberger, P. Gamnitzer, Ch. Föorster and E. Ramm: Large deformation fluid structure interaction - advances in ALE methods and new fixed grid approaches. In: *Fluid-Structure-Interaction: Modelling - Simulation - Optimization. Bungartz, H.-J., Schäfer, M. (eds.).* Lecture Notes in Computational Science and Engineering Vol. 53. Springer 2006.

[5] Ch. Förster, S. Genkinger, M. Neumann, W.A. Wall, E. Ramm: Fluid-Structure Interaction of Incompressible Flows and Slender Structures. *In: Multifield Problems in Solid and Fluid Mechanics, Helmig, R., Mielke, A., Wohlmuth, B.I. (eds.*), Lecture Notes in Applied and Computational Mechanics Vol. 28, Springer 2006, 187-218.

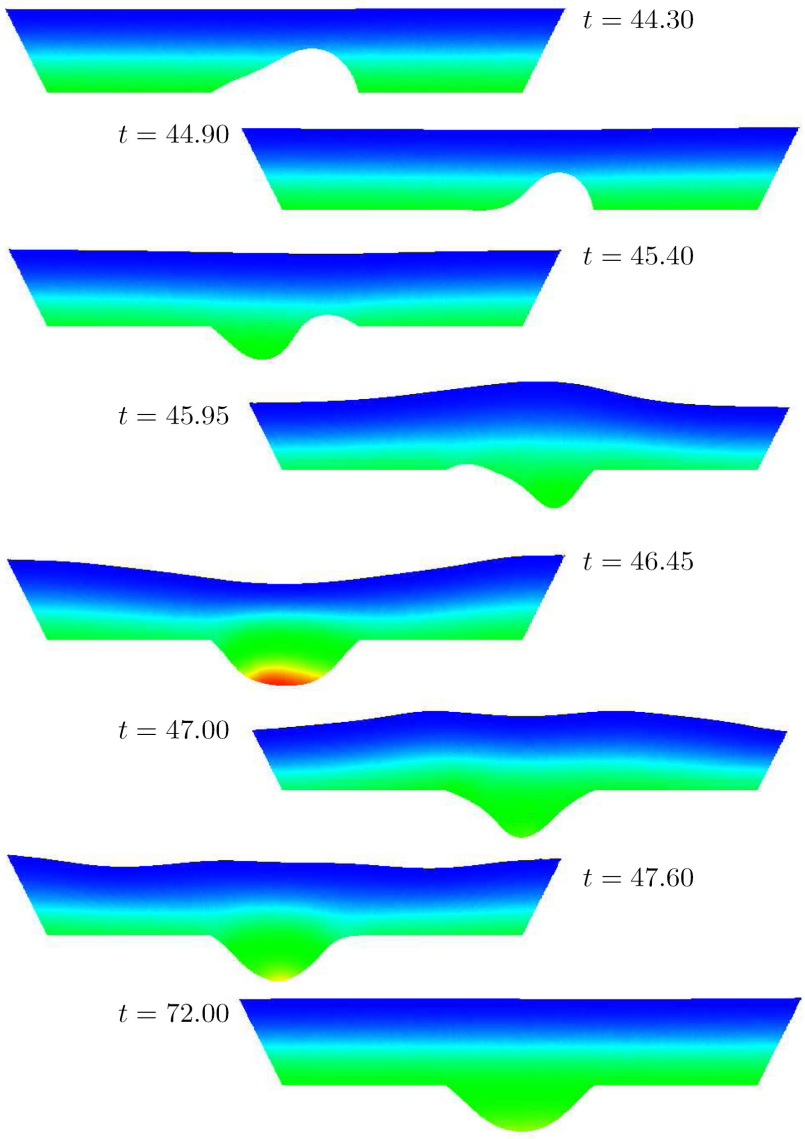

Figure 5: Basin with elastic arch: Collapsing arch with computed pressure solution.

Proceedings of the 6th International Conference on
Computation of Shell and Spatial Structures
IASS-IACM 2008: "Spanning Nano to Mega"
28-31 May 2008, Cornell University, Ithaca, NY, USA
John F. ABEL and J. Robert COOKE (eds.)

Full SPH modeling of the dynamic failure of shells interacting with a fluid

Alain COMBESCURE*, Farid ABED MERAIM, Bertrand MAUREL

*LaMCoS INSA Lyon UMR CNRS 5259
18-20 Allée des sciences 69621 Villeurbanne Cedex (France)
alain.combescure@insa-lyon.fr

Abstract

This paper is devoted to full SPH fluid-shell structure interaction. This formulation has been developed to easily treat the fracture under impact loads of shells filled with fluid. This method allows predicting the leakage rates in this type of crash. SPH is based on strong form of equilibrium equations. As all SPH solid formulations this shell formulation is subjected to tensile instabilities which are worse for shells than for usual solids. The proposed formulation is based on a total Lagrangian formulation which has the advantage to guarantee the stability and also to avoid the time consuming search of neighbor particles at each time step. The connectivity table is changed only when a fracture appears. A generalized stress model is used for plasticity and a fracture criterion is added to develop cracks. The fluid formulation is an updated Lagrangian formulation. The interaction is treated using pinball method. Some academic examples are presented as well as a comparison to an experiment.

1. Introduction

The simulation of shell fracture is not obvious especially if this shell is filled with fluid. A first modeling possibility is to use standard shell finite elements associated to an elastoplastic damage model. When the damage is high enough in an element it is simply deleted and the computation continues. This method is very popular especially in explicit codes, but it has two drawbacks:

-the model is not converging when the meshes are refined and that the failure propagation is most of time inconsistent with experimental results.

-in case of shells filled with fluid the prediction of leakage consecutive to a failure of the shell is not good.

A second approach is to rely on shell X-FEM technology. These methods are rather good for static and dynamics crack propagation simulations but the association with fluid leakage prediction is not easy because the fracture surface is not explicit in these formulations.

This paper is based on a full SPH of both fluid and structure, which greatly simplifies the fluid structure interaction

2. SPH formulation

The SPH method used for solid representation has to be consistent as well as stable. The consistency requirement is achieved by use of the use of extra "stress" points and for shells adding MLS shape functions. The stability is based (as proposed by T Belytschko and co-workers [1]) on a total Lagrangian formulation. A very small amount of artificial viscosity is added to harden the stability in case of severe impact loadings.

An original Reissner Mindlin MLSPH formulation is then proposed which is stable and consistent. The thick (and also thin) shell is modelled with only one layer of "particles" [4]. The consistency is here more difficult to address because of the shear and bending properties of the medium. The stability is also more difficult to control especially in case of shock loads. A simple solution is proposed. The proposed formulation is developed in

elasto-plasticity based on Ilyushin [2] and Crisfield theory of generalised plasticity. A very simple rupture criterion is proposed. The SPH shell theory used in this paper is fully developed in Maurel [4].

A typical example is displayed in figure 1 which compares the deformed shells after an impact for two computations: the first is done with MITC4 usual shell model the second is the same simulation with SPH shell formulation.

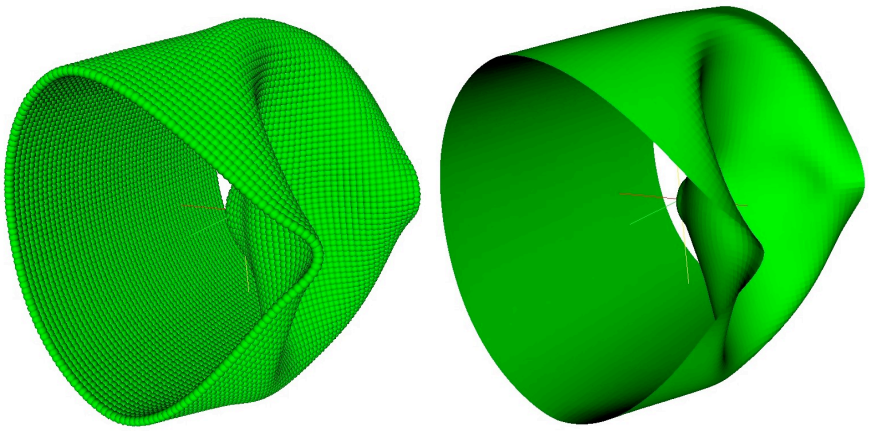

Figure 1 SPH deformed Shell MITC4 Deformed shell

Figure 2 displays a typical perforation prediction with SPH shell formulation.

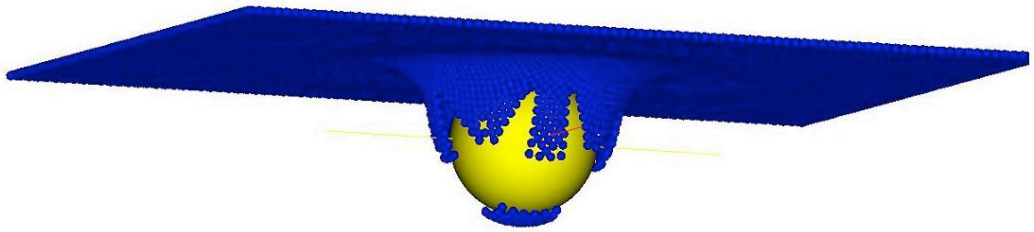

Figure 2: Shell SPH perforation example.

The fluid SPH method is based on the usual fluid updated Lagrangian formulation [5].

3. Interaction formulation

The interaction is treated with the pinball method [6] to avoid the air cushion effects which result from the so called “natural” method. The implementation in an explicit dynamics formulation needs to be handled with care in order to avoid artificial rebounds. The details of the contact algorithm can be found in [7]. A typical academic fluid structure interaction case is presented on figure 3 which compares the same application case in which the fluid is treated with SPH fluid particles and the solid is meshed with MITC4 shell elements on one side and with SPH Shell in the other case. The comparison is rather good.

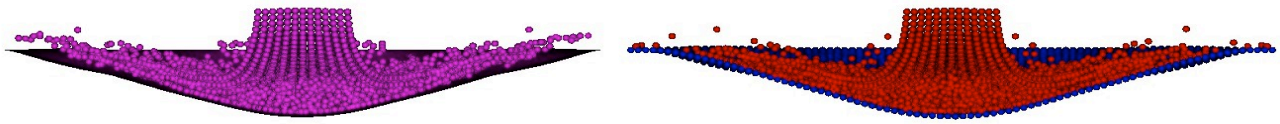

Fluid SPH Shell FE Fluid SPH Shell SPH

Figure 3: Academic example of fluid structure impact.

4. An original experiment and its interpretation

An original experiment was designed to validate the numerical modelling using full SPH modelling. A mass of 245Kg is launched at a variable speed on a piston filled with water as displayed on figure 4.

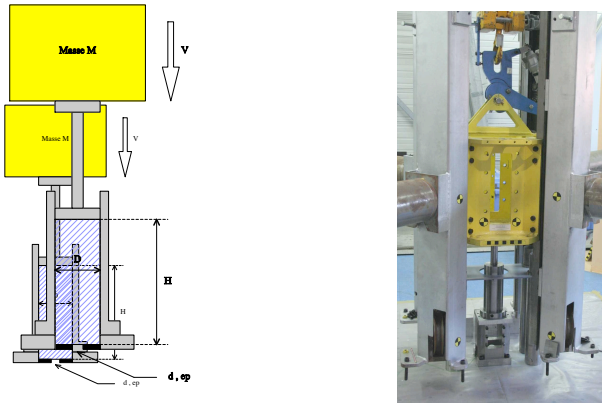

Figure 4: Piston geometry and photograph

This generates a pressure wave which breaks the bottom circular plate. 15 experiments with different disk geometries have beeeb tested. The most simple one is presented here: the disk has an initial hole of 20mm diameter (initially closed by a thin rubber membrane that breaks as soon as the pressure pulse reaches the bottom of the piston). The falling mass has a speed of 5m/s. The observed fluid jet shows typical repetitive bubbles as it can be onserved on figure 5.

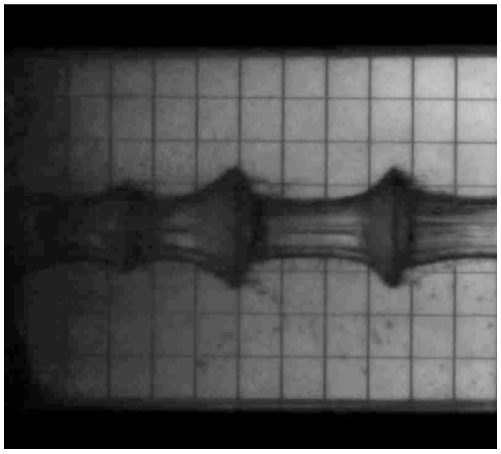

Figure 5: Experimental typical bubbles in fluid jet

The origin of these bubbles is not yet well understood but is reproduced qualitatively by the SPH model. (figure 6) flow has a constant speed of 92m/s. The measurement of the fluid velocity is obtained from a fast imaged film. The experiment is modelled with a full fluid shell sph model. Figure 6 gives the SPH Model which has about 12000 fluid particles and 1000 shell ones.

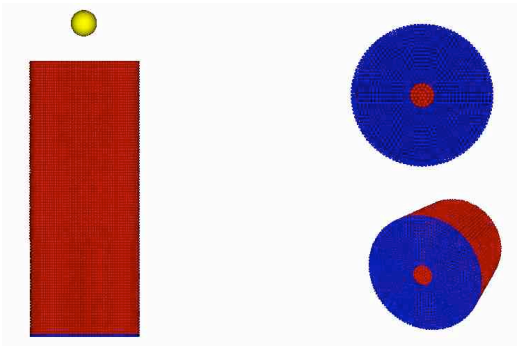

Figure 6: SPH Shell-fluid model

The computed jet is displayed in figure 7. One also sees the bubles in the computed jet. The computed jet velocity is 96m/s. One also has the velocity of the falling mass, from which one can compute the fluid volume variation. The resulting jet velocity is 20% smaller then the experimental one. This is due to the fact that the jet diameter is smaller than the hole size: this is also observed in the computations.

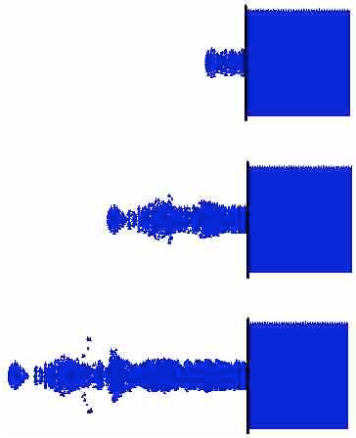

Figure 7: Computed fluid jet

References

[1] T Belytschko and Y Guo and W K Liu and S P Xiao, A unified stability analysis of meshless particle methods, *International Journal for Numerical Methods in Engineering*, 40,(2000), 1359-1400

[2] Ilyushin A A, Plasticité, Eyrolles, 1956

[3] T Rabczuk and P M A Areias and T Belytschko, A mesh free method for non-linear dynamic fracture, *International Journal for Numerical Methods in Engineering*, in press

[4] Maurel B, A Combescure, An SPH shell formulation for plasticity and fracture analysis in explicit dynamics, *International Journal for Numerical Methods in Engineering*, in press

[5] Letellier A. Contribution à la modelisation des impacts d'oiseaux sur des aubes de réacteur d'avion. PHD Thesis N° : 96-EVRY 0008 1996

[6] Belytschko T, Mac Neal O, Contact-impact by the Pinball method with penalty and Lagrangian Method. *International Journal for Numerical Methods in Engineering*, Vol 31, 1991, 547-572

[7] B Maurel, Modélisation par la méthode SPH de l'impact d'un réservoir rempli de fluide. PHD INSA 2008-ISAL-005

Proceedings of the 6th International Conference on
Computation of Shell and Spatial Structures
IASS-IACM 2008: "Spanning Nano to Mega"
28-31 May 2008, Cornell University, Ithaca, NY, USA
John F. ABEL and J. Robert COOKE (eds.)

Fluid-shell coupled simulation of supersonic disk-gap-band parachutes

Konstantinos KARAGIOZIS*, Ramji KAMAKOTI*, Carlos PANTANO*, Fehmi CIRAK**

*University of Illinois at Urbana-Champaign
Department of Mechanical Science and Engineering, Urbana, IL 61801, USA
** University of Cambridge, fc286@cam.ac.uk

Abstract

The development of new entry-descent-landing sequences for planned heavy payloads to be sent to Mars requires the use of new larger supersonic parachutes. The performance envelopes of these supersonic disk-gap-band (DGB) parachutes are presently not well understood. We developed a unique numerical solution strategy for simulating DGB parachutes by combining several novel developments in membranes, fluid-membrane interaction, fluid dynamics and block-structured mesh adaptation. The components of this solution strategy are as follows:

• Cable and membrane finite elements with unrestricted finite kinematics for simulating the parachute and 3-D rigid bodies for simulating the dynamics of the payload [1].

• High-resolution shock capturing finite difference method for simulating the supersonic flow field around parachute-payload system [2].

• Solution adaptive, dynamic mesh refinement for the flow field [3].

• An implicit geometry fluid-structure coupling methodology that embeds the structural system into a fixed Cartesian fluid mesh and continuously exchanges coupling data on the topological surface of the parachute-payload system between the fluid and solid solver components [4, 5].

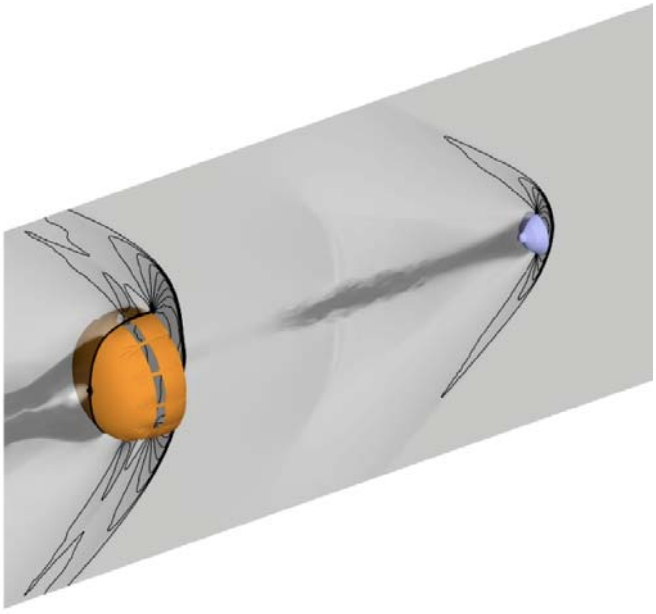

References

[1] F. Cirak and M. Ortiz. "Fully C^1-conforming subdivision elements for finite deformation thin-shell analysis". *Int. J. Numer. Methods Engrg.* , Vol. 51, 813–833, 2001.

[2] C. Pantano, R. Deiterding, D.J. Hill and D.I. Pullin. "A low-numerical dissipation patchbased adaptive mesh refinement method for large-eddy simulation of compressible flows". *J. Comput. Phys.* , Vol. 221, 63–87, 2007.

[3] R. Deiterding. "AMROC - Blockstructured adaptive mesh refinement in object-oriented C++ ". *Available at http://amroc.sourceforge.net.*

[4] F. Cirak and R. Radovitzky. "A Lagrangian-Eulerian shell-fluid coupling algorithm based on level sets". *Comp. & Struct.* , Vol. 83, 491–498, 2005.

[5] F. Cirak, R. Deiterding and S.P. Mauch. "Large-scale fluid-structure interaction simulation of viscoplastic and fracturing thin-shells subjected to shocks and detonations". *Comp. & Struct.* , Vol. 85, 1049–1065, 2007.

Proceedings of the 6th International Conference on
Computation of Shell and Spatial Structures
IASS-IACM 2008: "Spanning Nano to Mega"
28-31 May 2008, Cornell University, Ithaca, NY, USA
John F. ABEL and J. Robert COOKE (eds.)

Strongly coupled approach for the treatment of the fluid-structure interaction problems involving highly deformable solids and shells

R. Rossi*, P. Ryzhakov, E. Oñate

*International Center for Numerical Methods in Engineering (CIMNE)
Gran Capita' S/N (Campus Nord UPC), 08035, Barcelona,
rrossi@cimne.upc.edu

Abstract

The Interaction of fluids with the surrounding structures constitutes a classical challenge for the different numerical techniques. The recent theoretical developments in the field opened the way to new research lines to be investigated both from a theoretical and a practical point of view. The aim of current work is therefore twofold: first we will provide a simple theoretical explanation of the problems to be faced in incompressible FSI, later we will introduce and justify two procedures for the solution of complex interaction problems, a first one based on a monolithic approach (for the "quasi-incompressible" case) and the second on an efficient "stabilized" pressure splitting technique. The first of the two is applied in a lagrangian context while the second is considered for "standard" eulerian FSI.

1. Introduction

The numerical solution of coupled FSI problems represents a long standing problem for the numerical community since it involves the interaction between two fields which are typically treated using very different numerical techniques.

To face the challenge it is convenient to start by considering the features which are common to the structural problem and to the fluid problem, namely the dynamic equilibrium and the mass conservation.

In the case in which the structure is "compressible" while the fluid domain is incompressible and treated with equal order velocity-pressure elements a further issues rises due to the fact that the mass conservation is included in the equilibrium equation for the structure but treated as an external constraint inside the fluid domain. A monolithic formulation, involving both velocity and pressures as primary variables is still possible in this case but encounters additional difficulties connected to the need of introducing a stabilization for the velocity pressure problem (if linear elements are chosen).

Many possibilities exist to face this problem. This work will present two different approaches which are currently being developed at CIMNE to deal with problems of different type.

In particular, with the aim of describing the interaction of objects with flows involving free surface effects, a lagrangian approach for the description of the evolution of the fluid domain presents many advantages. Following the success of some SPH approaches we investigated in detail the possibility of including some weak compressibility in the fluid domain with the aim of improving the behavior of the PFEM (Idelsohn and Oñate [1]) for complex interaction problems. The most important advantage in this case Is the possibility of defining a monolithic, locking free, displacement-only formulation for the coupled FSI problem. Such a formulation is useful in following the interaction of the fluid flow with light weight structures as it presents excellent features in terms of both robustness and mass conservation.

As a second approach, aimed to the description of fully incompressible strongly coupled problems, a "standard" pressure splitting algorithm, written in ALE approach is described. In this case the strong coupling is achieved through the strongly coupled solution of the mass conservation equation and of the structural equation following the work of Rodriguez et al. The convergence of the iterations is guaranteed by the definition of a suitable modification for the pressure laplacian operator which allows to define an approximate "tangent operator" for the iterative loop between the structure and the pressure equation.

2. Applications

The approaches presented were applied to a number of different problems both at the level of "test cases" and of problems of real engineering interest.

The fully incompressible approach on the other hand allows the efficient solution of classically challenging problems such as the interaction of inflatable structures with the surrounding domain. Given its close relation to the fractional-step approaches and the good convergence for the inner loop, the method is extremely efficient from a computational point of view and is very promising in particular in view of its application in conjunction with semi-explicit fractional step algorithms (which are commonly used for large scale problems).

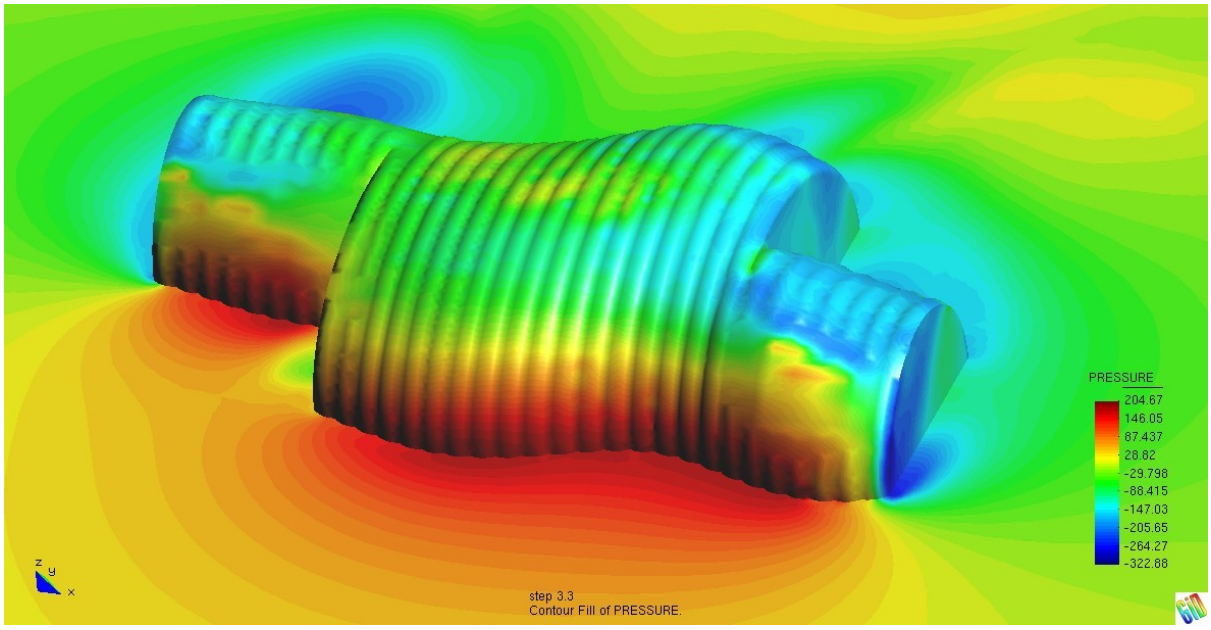

As an example the Lagrangian approach allows to treat satisfactorily the interaction between a thin membrane and the surrounding fluid taking in account correctly its flotation and the moment at which it passes from being completely submerged and being just partially submerged.

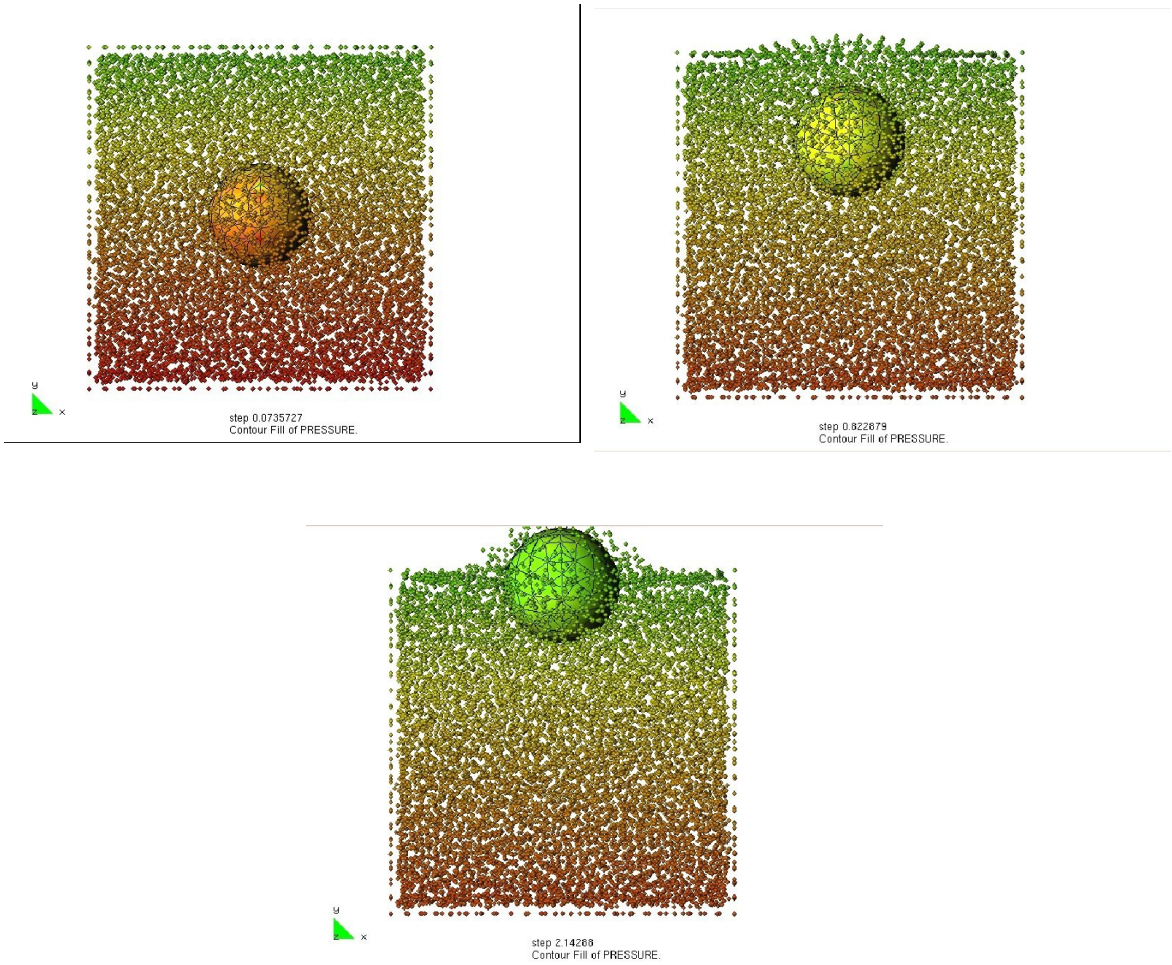

2. Conclusions

Two possible approaches to FSI were presented and discussed in their application to problems of real interest. The Lagrangian method is designed for the simulation of flows on rapidly varying domains and performs satisfactorely for problems featuring violent variations in the position of the free surface. The second technique is suitable for application to a different range of problems, in the domain of “standard” eulerian approaches. In this context it allows a very efficient solution and is competitive with the state of the art in the field.

References

[1] E. Onate, S.R. Idelsohn, F. Del Pin, R. Aubry, The particle finite element method. An overview, International Jour. Of Computational Methods, Vol. 1 n2, 267-307, 2004

Proceedings of the 6th International Conference on
Computation of Shell and Spatial Structures
IASS-IACM 2008: "Spanning Nano to Mega"
28-31 May 2008, Cornell University, Ithaca, NY, USA
John F. ABEL and J. Robert COOKE (eds.)

Numerical simulation of fluid-structure interaction for wind-induced dynamic response of cylindrical steel tanks with a dome roof

Zhen-Hua LIU *, Qi-Lin ZHANG, Ying ZHOU

*School of Civil Engineering, Shandong University, Jinan 250061, P. R. China
finliu@sdu.edu.cn

Abstract

Considering the fluid-structure interaction between wind flow and structure, the wind-induced dynamic responses of the dome roof and the cylindrical part are calculated by ADINA-FSI in this paper. The wind-induced dynamic coefficient and the distribution of pressures in the cylindrical part and in the roof of the tank are obtained, enabling designers to estimate wind load on structure shortly and conveniently in the engineering practice.

1. Introduction

The instability of cylindrical steel tanks under wind loads is of considerable interest in many parts of the world. Evidence is presented and arguments are advanced to support the proposition that vibration induced by turbulence in the air stream plays a significant role in initiating the collapse of steel oil storage tanks in high winds. An experimental strategy is often used to evaluate the response of steel tanks, but the wind tunnel experiments are often expensive. Nowadays, computational tools such as CFD, CSD and FSI(Robert Kroyer[1]) are used to investigate the performance of the flow and the response of the structures.

Interactions between a flexible structure and a contiguous fluid flow are of critical importance in many engineering problems. ADINA is a commercial finite element package which is especially suitable for problems with fluid-structure interactions(Dalin Tang et al.[2][3]). One of the important features of ADINA FSI analysis is the separate finite element discretizations for the solid domain and the fluid domain along the fluid-structure interface, which is particularly important for turbulent flows. In this paper, a numerical simulation of fluid-structure interaction for wind-induced dynamic response of the steel oil storage tanks was presented.

2. Description of Cylindrical Steel Tanks with a Dome Roof

A isolated tank[Fig1][Fig2][Fig3] whose axonometric drawing is shown as below was simulated numerically in this paper. The steel oil storage tank's diameter and height are 31.2m and 17.69m respectively. The height of the cylindrical part of the simulated tank is 14.274m. The thickness of the tank shell are varied from 18mm at the downward side of the cylindrical part to 11mm at the upward side of the cylindrical part. Besides, the dome roof's thickness is 15mm.

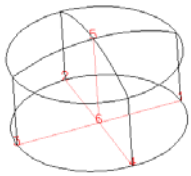

Figure 1 the tank

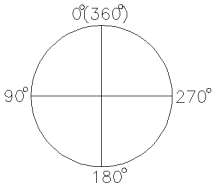

figure 2 the top view of the tank

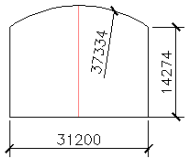

figure 3 the front view of the tank

2.1 The structure model

In FSI analysis of the tank with a dome roof, the geometrical nonlinear, isotropy-elastic, large-displacement and small-strain materials are considered in the finite element model which accords with the reality and can be the reference of practical projects. The structure model[fig4]is shown. The material of the steel oil storage tank is elastic model whose elastic modulus E and Poisson's ration γ_1 are $2.06\times10^{11}N/m^2$ and 0.3 respectively. The cylindrical part of the tank is simulated by 5 different surfaces due to their different thicknesses. In the finite element model, the cylindrical part shell and dome roof shell are discretized by 4-node shell element in ADINA software.

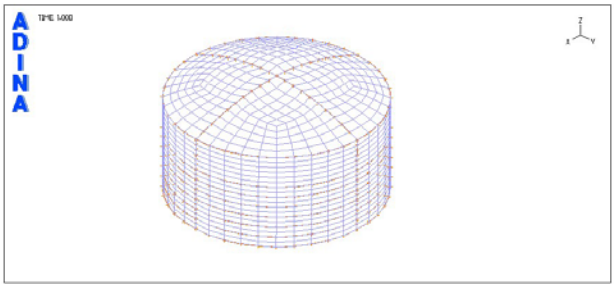

Figure 4 the structure model of the tank

2.2 The fluid model

The dimension of the computational flow domain is $440m\times220m\times68.274m$, and the windward of the steel oil storage tank locates 98.696m away from the inlet of flow and the leeward of which locates 310m away from the outlet of the simulated wind tunnel. The fluid is modeled using the viscous and incompressible Navier-Stokes equations with $k-\varepsilon$ turbulence model(K.J. Bathe[4])(ADINA corp.[5]). The flow domain is discretized by 8 nodes hexahedron FCBI-C fluid element. The $x\times y\times z$ meshes used for fluid are $(7+1+35)\times(10+10+10)\times(10+4+8)$ with finer meshes near the structure.

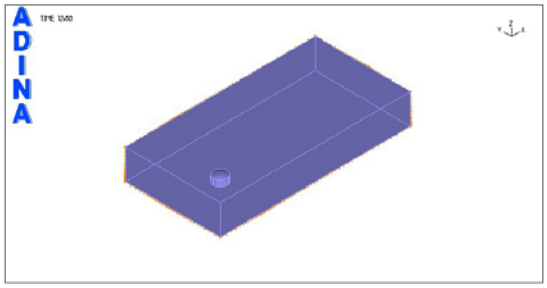

Figure 5 the perspective view of the fluid model

2.3 The numerical simulation results

The model was solved using ADINA which is a finite element package capable of solving a wide range of solid and fluid mechanics engineering problems. The governing finite element equations for the solid and the fluid were solved by Full-Newton iteration and Newton iteration respectively. The fluid-structure interaction solution is obtained by the iterative computing. The fully coupled response is calculated. The results reveal the velocity in the flow domain, and typical features of the structure such as displacements, velocity and acceleration are obversed. Furthermore, the wind-induced dynamic coefficients and the distributed wind pressure coefficients are calculated from the displacements and reaction forces of the nodes in the structure model(Xinli Chen et al.[6]).

In Fig.6 x-direction wind velocity contour-line on the y=0m cut section of the fluid domain is shown. The magnitude of the velocity behind the leeward is small. Fig.7 shows the x-velocity vector on the y=0m cut section near the cylindrical steel tank with a dome roof. It is obvious that there are vortexes behind the leeward.

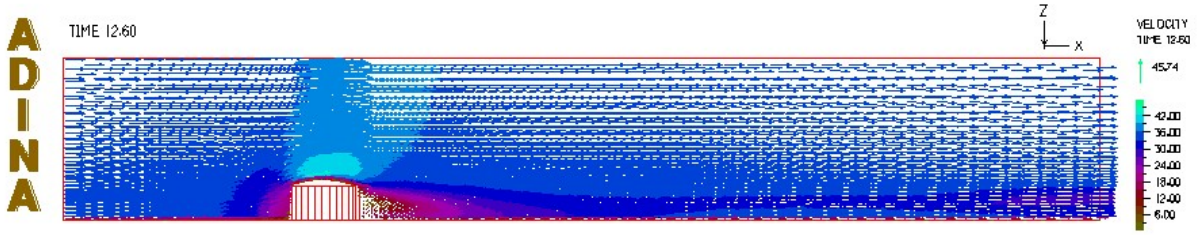

Figure 6: X-direction wind velocity contour-line on the y=0m cut section

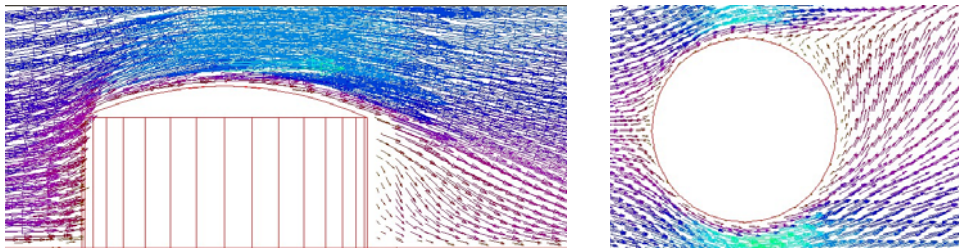

(a) details of the x-direction wind velocity contour-line on the y=0m cut section

(b) details of the velocity contour-line at the height of H=10m.

Figure 7: Details of the velocity band around the cylindrical steel tank

According to the results, the time-dependent displacement of the structure is known, and from which the wind-induced dynamic coefficient can be calculated, and the wind-induced dynamic coefficients of the cylindrical part and the dome roof of the cylindrical steel tank are 2.2 and 3.5 respectively.

The distributed pressure coefficient contour lines of the 4 zones of the cylindrical part and the dome roof of the tank are shown in Fig.8 and Fig.9.

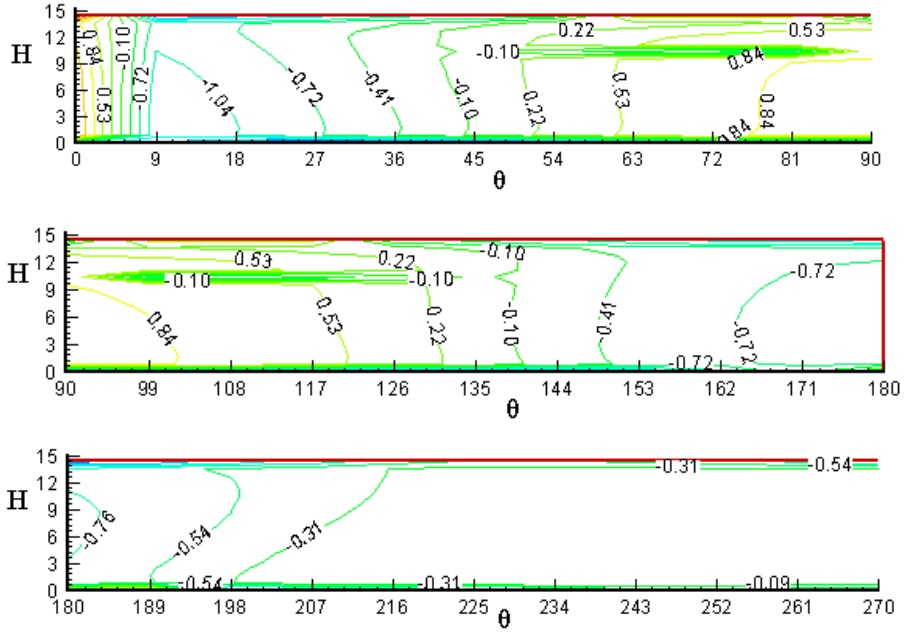

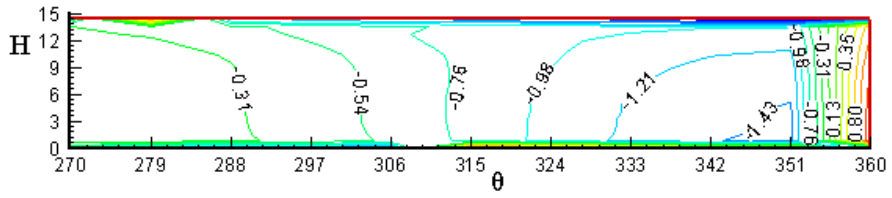

Figure 7: Distributed pressure coefficient contours of the cylindrical part

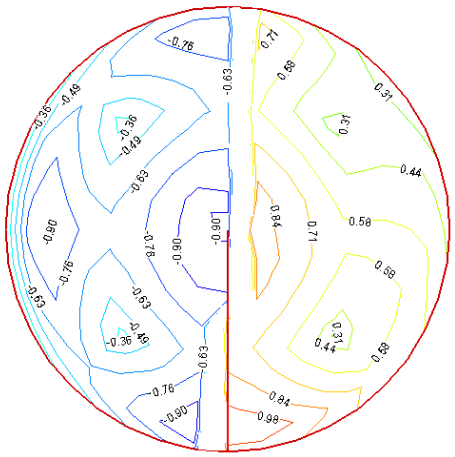

Figure 8: Distributed pressure coefficient contours of the dome roof

3. Conclusion

It is concluded that the wind induced dynamic coefficient and the wind pressure distribution coefficients of the cylindrical steel tanks with a dome roof is different from which of other forms of structures(Construction Industry Press[7]). And the wind pressure distribution coefficients are also different among different parts of the cylindrical part. When engineers begin designing cylindrical steel tanks, they must consider different wind induced dynamic coefficients and wind pressure distribution coefficients of the different patterns of the tanks. Further research about the tank groups subjected to the action of the wind will be taken in the future.

References

[1] Robert Kroyer, “FSI analysis in supersonic fluid flow”, Computers and Structures 81(2003) 755-764.

[2] Dalin Tang, Chun Yang, David N. Ku, “A 3-D thin-wall model with fluid-structure interactions for blood flow in carotid arteries with symmetric and asymmetric stenoses”, Computers and Structures 72(1999) 357-377.

[3] Dalin Tang, Chun Yang,Yan Huang, David N. Ku, “Wall stress and strain analysis using a three-dimensional thick-wall model with fluid-structure interactions for blood flow in carotid arteries with stenosed”, Computers and Structures 72(1999) 341-356.

[4] K.J. Bathe. Finite Element Procedures. Prentice-Hall, Inc., 1996.

[5] ADINA Theory and Modeling Guide Volume III□ADINA-F,Report ARD 04-09,2004.

[6] Xinli Chen, Shizhao Shen, Yang Xiang.Wind-inducing Response Analysis and The Coefficient for Wind-Resistant Design of The Saddle-Shaped Membrane Structures. Journal of Tianjin Institute of Urban Construction 2001:7(3): 159-163.

[7] Load Code for Building Structures(GB50009-2001). Beijing: Construction Industry Press of China,2002.